Global Seasonal Precipitation Anomalies Robustly Associated with El Niño and La Niña Events—An OLR Perspective*,+

ANDREW M. CHIODI AND D. E. HARRISON

Joint Institute for the Study of the Ocean and Atmosphere, University of Washington, and NOAA/Pacific Marine Environmental Laboratory, Seattle, Washington

(Manuscript received 30 May 2014, in final form 17 April 2015)

ABSTRACT

El Niño–Southern Oscillation (ENSO) events are associated with particular seasonal weather anomalies in many regions around the planet. When the statistical links are sufficiently strong, ENSO state information can provide useful seasonal forecasts with varying lead times. However, using conventional sea surface temperature or sea level pressure indices to characterize ENSO state leads to many instances of limited forecast skill (e.g., years identified as El Niño or La Niña with weather anomalies unlike the average), even in regions where there is considerable ENSO-associated anomaly, on average. Using outgoing longwave radiation (OLR) conditions to characterize ENSO state identifies a subset of the conventional ENSO years, called OLR El Niño and OLR La Niña years herein. Treating the OLR-identified subset of years differently can both usefully strengthen the level of statistical significance in the average (composite) and also greatly reduce the year-to-year deviations in the composite precipitation anomalies. On average, over most of the planet, the non-OLR El Niño and non-OLR La Niña years have much more limited statistical utility for precipitation. The OLR El Niño and OLR La Niña indices typically identify years in time to be of use to boreal wintertime and later seasonal forecasting efforts, meaning that paying attention to tropical Pacific OLR conditions may offer more than just a diagnostic tool. Understanding better how large-scale environmental conditions during ENSO events determine OLR behavior (and deep atmospheric convection) will lead to improved seasonal precipitation forecasts for many areas.

1. Introduction

Definitions for the warm (El Niño) and cold (La Niña) phases of El Niño–Southern Oscillation (ENSO) based on tropical Pacific surface marine conditions have been used previously to reveal the now well-known statistical links between ENSO and seasonal weather anomalies around the globe [see, for example, the seminal seasonal precipitation and temperature composites described by Ropelewski and Halpert (1986, 1987, 1989) and Halpert and Ropelewski (1992)]. These links provide an important basis for skillful statistical seasonal weather prediction where they are strong enough (Kiladis and Diaz 1989; Smith et al. 1999; Wolter et al. 1999). It has become clear, however, that even in the most strongly affected regions, many years identified as El Niño or La Niña, based on the now commonly used SSTA-based ENSO definitions, do not have seasonal weather anomaly patterns that match those seen on average (e.g., Harrison and Larkin 1998; Larkin and Harrison 2005a,b). Seasonal weather anomalies may not in general be simply and strongly related to ENSO (Kumar et al. 2007) as it has been conventionally defined. We show here that a different perspective on ENSO conditions can improve the statistical weather associations on which much seasonal forecasting is based.

Outgoing longwave radiation (OLR), sea level pressure (SLP), and sea surface temperature (SST) all provide measures of the state of the coupled-ENSO system, but of these OLR has the closest connection to the atmospheric heating anomalies that drive atmospheric

* Joint Institute for the Study of the Ocean and Atmosphere Contribution Number 2068 and NOAA/Pacific Marine Environmental Laboratory Contribution Number 3946.
+ Supplemental information related to this paper is available at the Journals Online website: http://dx.doi.org/10.1175/JCLI-D-14-00387.s1.

Corresponding author address: Andrew Chiodi, JISAO University of Washington, 7600 Sand Point Way NE, Seattle, WA 98115.
E-mail: andy.chiodi@noaa.gov

DOI: 10.1175/JCLI-D-14-00387.1

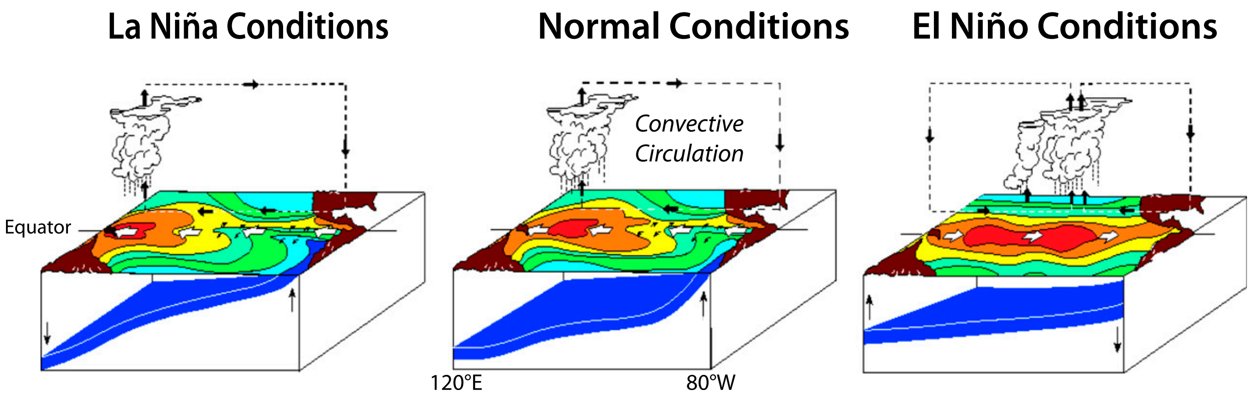

FIG. 1. The familiar ENSO cartoons, illustrating the subsurface (thermocline) surface (SSTA, SLP, and near-surface winds) and atmospheric convection conditions commonly associated with (left) La Niña, (center) ENSO-neutral, and (right) El Niño states.

circulation anomalies elsewhere. Direct measurements of atmospheric heating anomalies are not currently available. Heating estimates may be obtained from some atmospheric models and reanalyses, but the extent to which the present generation of climate models properly reproduces ENSO physics is not clear; also, there are likely large differences in model-produced heating, given the models' differing kinematic behavior. Thus, we turn to OLR to seek better understanding of how the behavior of tropical Pacific atmospheric heating anomalies relates to the seasonal weather anomalies observed during El Niño and La Niña years.

OLR in the deep tropics is strongly influenced by the presence or absence of deep atmospheric convective activity. It is a common belief that tropical Pacific deep atmospheric convective activity spreads eastward during the transition to El Niño state (as depicted in the familiar ENSO cartoons; see Fig. 1). Chiodi and Harrison (2010) looked for this spread in convection using OLR. They found that the strikingly low-OLR anomalies that are indicative of significant amounts of tropical deep atmospheric convective activity are clearly seen in the eastern central Pacific during some, but not all, of the years that are identified as El Niño years, based on the commonly used SST anomaly (SSTA)-based ENSO definitions. This type of OLR behavior is unique to this subset of years. Whereas ENSO SSTA (e.g., the Niño-3.4 index) follows a continuous distribution, the negative OLR peaks seen in these years are well separated from the background variability seen in this region at other times (see Chiodi and Harrison 2008, 2010; also Fig. 5a in section 3, below). Thus, the OLR El Niño index clearly picks out a subset of the commonly identified years.

With focus on the United States, Chiodi and Harrison (2013) showed that the years identified by the OLR El Niño index yield composite seasonal weather anomalies with familiar patterns (broadly resembling those described in earlier ENSO studies), high levels of statistical significance, and strong year-to-year consistency. Composites based on all of the years commonly identified as El Niño were also shown to have patterns shaped like those seen in the OLR El Niño composite, but at considerably weaker amplitude. Composites based just on the other non-OLR El Niño years produced seasonal weather anomalies with very little statistically significant anomaly over the United States and a high degree of year-to-year deviation. Thus, from a seasonal weather forecasting perspective, most of the useful impacts of El Niño on the United States are as a result of the years identified by the Chiodi and Harrison (2013) OLR El Niño index.

We herein identify a separate and novel OLR index for La Niña. Our earlier OLR El Niño index, which looks for the eastward spread in equatorial Pacific deep atmospheric convection that is specific to El Niño events, was not intended as a measure of changes associated with La Niña events. Thus, a different approach is needed in this case.

Our approach to identifying an OLR index for La Niña, described in more detail in section 2 below, was motivated by our phenomenological understanding of La Niña atmospheric convection conditions (e.g., Fig. 1) and their connection to the easterly wind events that have been shown to drive La Niña cooling of the oceanic waveguide (see Chiodi and Harrison 2015). Like its warm-ENSO counterpart, the OLR La Niña index (OLNI) rather clearly identifies a subset of the years with ENSO status based on the NOAA historical ENSO definition (5 consecutive months of the 3-month running average Niño-3.4 SSTA amplitude exceeding 0.5°C).

The sections of this paper are organized as follows. Section 2 describes the data and methods used, including the rationale behind our approach to identifying an

OLR index for La Niña (section 2c). Section 3 discusses the perspective on El Niño and La Niña offered by the respective OLR indices and compares this to the behavior of the more commonly referred to Niño-3.4 SSTA index. Composites of tropical Pacific OLR anomaly and global land precipitation anomaly based on the identified OLR El Niño and OLR La Niña years are discussed in section 4. Composites based on the other years that have ENSO status based on SSTA but not OLR are also discussed in section 4. Section 5 examines the question of whether our composite results can be explained by invoking a linear relationship with Niño-3.4 SSTA. Most of the OLR El Niño years and all of the OLR La Niña years were identified by their characteristic OLR behavior in time to be of use to boreal wintertime and later seasonal forecasting efforts. In section 6 we briefly explore the prospect of exploiting this observed feature of the OLR events to aid statistical forecasting of seasonal precipitation anomaly.

2. Data and methods

a. Precipitation and sea surface temperature data

Monthly mean Global Precipitation Climatology Centre (GPCC) precipitation data were obtained from the NOAA/Office of Oceanic and Atmospheric Research (OAR)/Earth System Research Laboratory (ESRL) Physical Sciences Division (PSD) located in Boulder, Colorado (available from their website at http://www.esrl.noaa.gov/psd/; Schneider et al. 2011). More information about this gauge-based gridded precipitation dataset is available from the GPCC homepage, (http://gpcc.dwd.de; see also Rudolf and Schneider 2005; Rudolf et al. 2010).

The SSTA data used herein (HadISST; Met Office Hadley Center 2003) were provided by the Met Office Hadley Centre. See Rayner et al. (2003) for discussion of the HadISST1 dataset.

b. OLR and the OLR El Niño index

We use daily interpolated OLR averages provided by NOAA/OAR/ESRL PSD (NOAA/NCAR 1996). This is a satellite-derived product available on a $2.5° \times 2.5°$ grid. Details of the interpolation technique are described by Liebmann and Smith (1996). Daily OLR averages are available from July 1974 to the present with a gap in coverage from March to December of 1978. Because of this gap, the 1978/79 period is omitted from consideration here.

For the post-1979 period, we have verified the results based on NOAA interpolated OLR data with a second set of results based on the High Resolution Infrared Radiation Sounder (HIRS) OLR climate dataset (Lee et al. 2007; Lee 2014), which provides daily averages of OLR beginning in 1979 (NOAA/NCDC 2014).

In the tropics, large shifts in the satellite-measured OLR are associated with transitions from relatively clear sky conditions, in which OLR is dominated by near-surface longwave radiation, to deep convective conditions, in which OLR is influenced mainly by radiation from the cooler deep cloud tops (e.g., Trenberth et al. 1998). Absolute OLR measurements less than $230\,\mathrm{W\,m^{-2}}$ have previously been used as a proxy for deep tropical convection (Garreaud and Wallace 1998), with values substantially larger than that indicative of a lack of deep atmospheric convective activity.

The Chiodi and Harrison (2013) OLR index for El Niño (as described in the introduction) is based on monthly OLR anomaly behavior averaged over the region bounded by 160°–110°W and 5°S–5°N. To calculate the OLR El Niño index, the daily average OLR data are first filtered with a 30-day running mean filter and anomalies are determined by removing the linearly interpolated climatological monthly average. A climatological base period of 1974–2011 (the study period comprising ENSO years 1974/75–2010/11) is used throughout this paper. We have confirmed that using the alternative HIRS OLR climate dataset (Lee 2014) instead of the NOAA interpolated OLR dataset to compute the OLR El Niño index does not qualitatively affect the results (plots of the index based on both datasets are overlaid in Fig. A1 of appendix A, for reference). We expect the HIRS dataset to be useful moving forward but base our results here mainly on the NOAA interpolated OLR dataset, since it is available beginning in 1974, whereas the HIRS version begins later, in 1979.

Here, ‘‘ENSO year’’ is taken as defined in previous compositing studies (Rasmusson and Carpenter 1982; Larkin and Harrison 2002), with year 0 typically corresponding to the onset and development of the mature stage of ENSO (e.g., 1997 of the large 1997/98 El Niño event) and year 1 the year following onset/development. Peak tropical Pacific anomaly conditions typically occur around the end of year 0 or beginning of year 1.

c. The OLR La Niña index

Conventional understanding of coupled ENSO dynamics (e.g., Fig. 1) posits that the western equatorial Pacific warm-pool region, which is normally characterized by vigorous deep atmospheric convective activity, experiences a decrease in convection (increased OLR) as the system transitions to La Niña state. To practically identify the equatorial oceanic region associated with this transition, we compute the difference between OLR

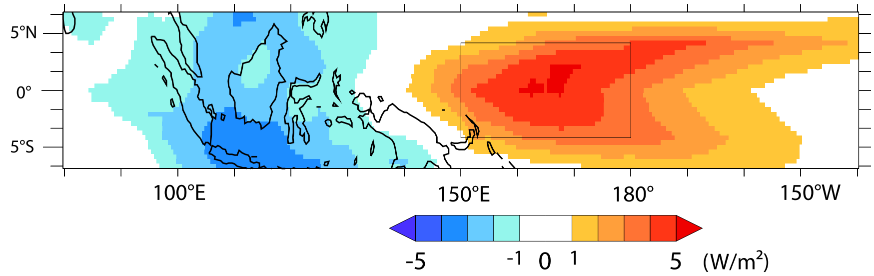

FIG. 2. Long-term-averaged change in OLR between La Niña minus ENSO-neutral conditions. To produce this figure, ENSO anomaly states were defined using a preliminary 0.75°C Niño-3.4 SSTA threshold (e.g., ENSO-neutral here defined as all times with |Niño-3.4 SSTA| < 0.75°C.

averaged over all times falling into the La Niña state minus the average over all ENSO-neutral times, with ENSO state preliminarily defined using Niño-3.4 SSTA. The region bounded between 150°E and 180° and between 5°S and 5°N is highlighted in this manner (Fig. 2). We take this region as the averaging region for our OLR La Niña index.

We focus on the synoptic scale behavior of OLR averaged over this 5°S–5°N, 150°E–180° region. Recent study of the role of equatorial Pacific easterly wind events in the onset and development of La Niña events motivates this approach. Specifically, it has been found that (i) easterly wind events, characterized by surface wind stress anomaly amplitudes greater than 0.045 Pa and average time scales (in an *e*-folding sense) of about one week are a prominent component of subseasonal zonal wind variability over the equatorial Pacific; (ii) single "easterly wind surges" drive a few tenths of a degree Celsius cooling, on average, over the Pacific Ocean waveguide; (iii) this cooling persists for 2–3 months after the wind surge subsides; (iv) the frequency of the easterly surges increases (roughly doubles) as ENSO SSTA cools, providing a positive feedback for La Niña development; and (v) a series of easterly surges that reflect their average rate of occurrence (~1 per month), including this increase in frequency, is sufficient to drive a La Niña in a realistic ocean general circulation model in the absence of other sources of forcing (Chiodi and Harrison 2015). In short, easterly wind surges are as important to La Niña as westerly wind events are to El Niño (cf. Harrison and Chiodi 2009; Chiodi et al. 2014).

We find that the occurrence of strongly positive, synoptic time–scale OLR anomalies over the western tropical Pacific warm-pool region are associated with subseasonal increases in easterly wind stress anomalies (Fig. 3). Thus, the accumulation of high-OLR days over this region is linked to integrals of easterly wind events, which can now be understood to be important to driving and maintaining La Niña surface cooling.

Informed by these findings, the OLR-based index we have chosen to examine for La Niña is based on the sum of strongly positive OLR (clear sky) days over the western tropical Pacific and the months typically

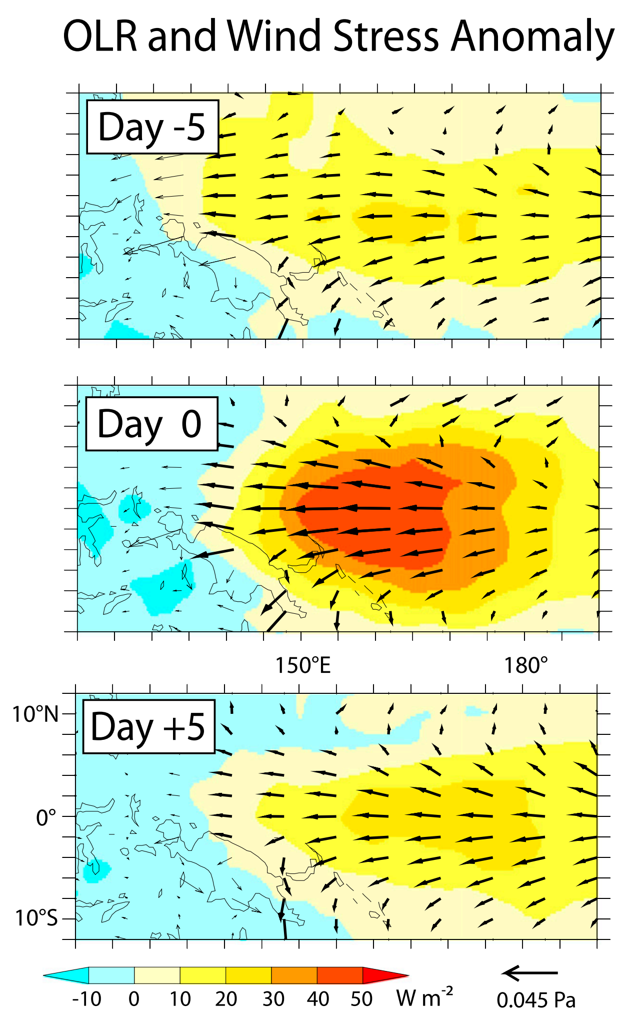

FIG. 3. (middle) Composites of OLR (shading) and surface wind stress (vectors) based on the occurrence of days with strongly positive OLR over the western tropical Pacific. Composites 5 days (top) prior to and (bottom) after the day with maximum OLR.

associated with La Niña onset and development. More specifically, the OLNI is defined based on daily average OLR conditions as

$$\mathrm{OLNI}(n) = \sum_{i=1}^{n} C(i),$$

with

$$C(i) = \begin{cases} 1, & \text{if } \mathrm{OLR}(i) > \mathrm{OLRc} \\ 0, & \text{otherwise} \end{cases},$$

where n and i are the number of days since 1 March of ENSO year 0 (the index running sum begins then, in each year); OLR(i) is the daily average OLR value averaged over the region bounded between 150°E–180° and 5°S–5°N; and OLRc is 260 W m^{-2}, which in this region is the 90th-percentile clear-sky value. The OLNI with n corresponding to 31 December of year 0 is shown in Fig. 4b (tops of bars). These seasons (March–December) are the ones in which La Niña onset and growth typically occurs (Larkin and Harrison 2002) and were those mainly considered in the easterly wind surge study of Chiodi and Harrison (2015).

Like its OLR El Niño counterpart (discussed in section 3) the OLNI exhibits a rather eventlike behavior in the sense that a handful of years stand out from the others. In this case (Fig. 4b), ranking each year by its end-of-calendar-year OLNI value identifies six years that stand out from the other years based on a discontinuity of about one-half of a time series standard deviation that exists between the lowest of the top six years (1998/99 has an index value of 67 days) and the next most highly ranked year, which reaches only 51 days (see Figs. 5b and 6). Below this level, the ranked-distribution of yearly OLNI values is basically continuous (the subsequent gaps between consecutively ranked values are <0.25 standard deviation).

For the purposes of this study, we define as OLR La Niña years the six years that exceed the 60-day threshold. The 60-day value is crossed only in these six years, even if the index is extended (n is increased) through May of ENSO year 1. The dates in which this index first crosses the 60-day threshold in each of these six years are listed in Table 1. In each case, the 60-day threshold is crossed by the end of November year 0, in time to be of use to December–February (year 0/1) and later seasonal forecasting efforts. The 30 November value in each of the OLR La Niña years is shown by the upper extent of light blue shading in Fig. 4b, for reference.

If the integral is stopped at the end of August in each year (in time to be of use to September–November forecasts), 3 of the 6 La Niña event years (1975/76,

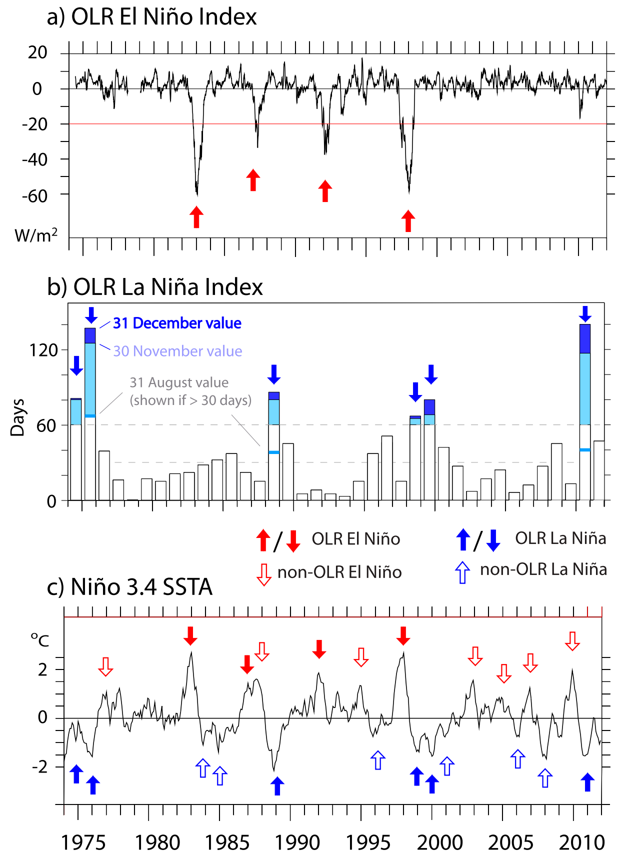

FIG. 4. (a) The Chiodi and Harrison (2013) OLR El Niño index, (b) the OLR La Niña index, and (c) Niño-3.4 region SSTA.

1988/89, and 2010/11) stand out (by >0.5 standard deviation) with respect to the other years integrated up to that same date. Thus, these 3 years could have been clearly identified in time to be of use to forecasting of the earlier September–November (year 0) season. The index value on 30 August of these 3 years is also marked in Fig. 4b.

Following Chiodi and Harrison (2013), we define as non-OLR La Niña years the other years that are identified as La Niña based on the current NOAA historical ENSO definition but that are not identified by the OLR La Niña index. There are also 6 such non-OLR La Niña years in the period considered (marked by unfilled blue arrows in Fig. 4c).

d. *OLNI parameter sensitivity*

We find that small changes in the index-averaging parameters, such as using the 95th-percentile daily OLR value (265 W m^{-2}) or 85th-percentile value (257 W m^{-2}) instead of the base-case 90th percentile, does not qualitatively change the results; although these changes change the scale of the index accordingly, the same six years are distinguished in each case.

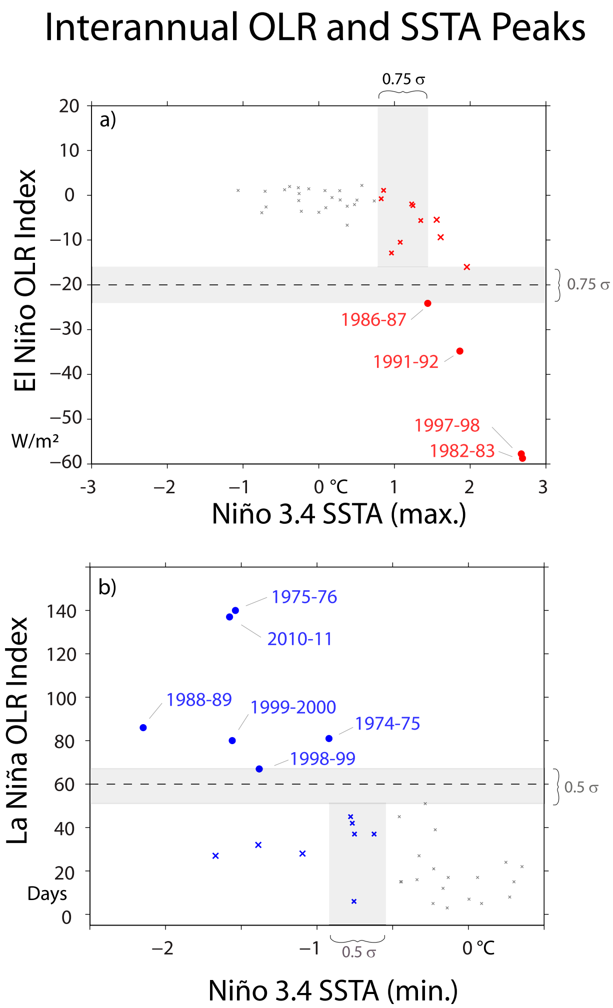

FIG. 5. (top) Minimum monthly average OLR El Niño index vs maximum monthly average Niño-3.4 SSTA seen each year (August–April 1974/75–2010/11). (bottom) OLR La Niña index (OLNI) vs minimum monthly average Niño-3.4 SSTA seen during the OLNI integration period. In each panel, the OLR-index values lying between the weakest event and closest nonevent are shaded. The equivalent distance (in std dev) behind the weakest-event SSTA peak is also shaded for reference.

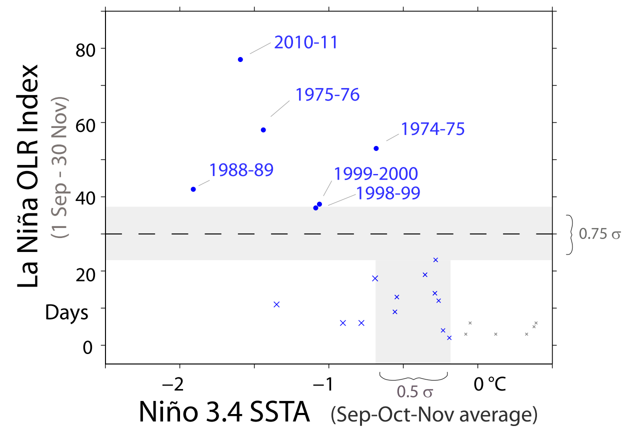

FIG. 6. As in Fig. 4b, except for OLNI integrated 1 Sep–30 Nov year 0 and September–November averaged Niño-3.4 SSTA.

We also find that small changes in the averaging region, such as using meridional bounds of 4° rather than 5° or going to 160°W rather than 180°, does not qualitatively change the results in the sense that the same six years are rather clearly distinguished in this case (i.e., a gap in the distribution of index values between the top six and other years remains in place in each case). Moving the western boundary slightly farther west (say to 145°E) also does not qualitatively alter the index.

Not all processes that affect OLR over the averaging region are involved in coupled ENSO dynamics. The Madden–Julian oscillation (MJO) is an eastward-propagating oscillatory feature of the tropical atmosphere with expression in OLR, including some phases associated with positive OLR over the western Pacific [e.g., the phases labeled 1 and 2 by the popular Wheeler and Hendon (2004) real-time multivariate MJO (RMM) definition]. We have found, however, very little correspondence between the years identified by our OLR index and those that are extreme in terms of MJO activity. For example, the MJO activity measure formed by summing in each year (over the same integration period) the number of days that the MJO is "active" (RMM amplitude >1; see Wheeler and Hendon 2004) and in phase 1 or 2 (the phases with most potential to trigger our index) has a correlation coefficient magnitude of only 0.01 with our OLR La Niña index. Year-to-year changes in this aspect of MJO activity are not what make the 6 OLR La Niña years stand out in terms of OLR behavior. The easterly wind anomalies seen in Fig. 3 signify that, on average, the conditions associated with the OLR index are associated with easterly wind stress anomalies that drive and maintain La Niña–type surface cooling of the equatorial Pacific.

It may be asked why our OLR La Niña index is based on synoptic-scale behavior, in contrast to our monthly mean OLR El Niño index. We have sought indices that identify OLR events as early in the calendar year as

TABLE 1. Dates on which the OLR La Niña index initially crossed the 60-day threshold.

ENSO year	1974/75	1975/76	1988/89	1998/99	1999/2000	2010/11
Date	Sep 1974	Jul 1975	Sep 1988	Nov 1998	Oct 1999	Sep 2010

possible, in order to take forecast advantage of the strong OLR-event/seasonal weather anomaly connections. These different perspectives make best use of the behavior of the tropical coupled ocean–atmosphere system in the year of the onset of each type of event to this end.

We have confirmed that using the HIRS OLR data as well as the NOAA interpolated OLR data in the post-1979 period results in the same subset of years being clearly identified over this period.

3. OLR indices

OLR behavior in the OLR El Niño index region is characterized by its eventlike distribution of interannual peaks (Fig. 4a), which is significantly different from the essentially continuous (Gaussian type) distribution seen among many of the commonly used ENSO indices, such as Niño-3.4 index and the Southern Oscillation index (see Chiodi and Harrison 2008, 2010, 2013). This eventlike behavior makes the determination of El Niño event status based on OLR much less ambiguous than when using the commonly used indices (Chiodi and Harrison 2008).

The interannual peaks seen in the OLR El Niño index (minima) and Niño-3.4 index (maxima) are plotted against one another in Fig. 5a, wherein a dashed line marks the suggested OLR El Niño event threshold of $-20\,\mathrm{W\,m^{-2}}$. The four large OLR events (red circles) have monthly average OLR peak amplitudes ranging from -24 to $-59\,\mathrm{W\,m^{-2}}$. The smallest of these, in terms of OLR, is 0.75 standard deviation removed from the next closest (negative) OLR peak seen in the other years. The four large OLR events occur in years with peak monthly average Niño-3.4 values between 1.4° and 2.7°C. The 2 years with the strongest SSTAs also have the largest OLR peaks. However, there are 3 other years (large red crosses) that have Niño-3.4 peaks that exceed 1.4°C but do not have OLR amplitudes that reach the OLR-event level. Additionally, there are 7 more years (small red crosses) that have Niño-3.4 peaks within 0.75 standard deviation of 1.4°C, which is the smallest Niño-3.4 peak seen among the four large OLR events. Based on SSTA alone, it is difficult to distinguish these 10 other years (red crosses) from the lesser 2 OLR El Niño years.

A companion plot of the OLNI values versus Niño-3.4 minima is shown in Fig. 5b. In this case, the 6 years identified as OLR La Niña events (OLNI $>$ 60 days; blue circles) have Niño-3.4 (negative) peaks in the range from $-0.9°$ to $-2.1°$C. No other years exceed the suggested OLR-event threshold. The spread between the smallest OLNI value seen among the 6 OLR La Niña years and the nearest non-OLR La Niña year is equivalent to 0.5 OLNI standard deviation. There are 3 non-OLR La Niña years (large blue crosses) that have negative Niño-3.4 peaks <-1.0°C (i.e., cooler than the smallest SSTA peak seen among the OLR La Niña events) and another 5 (small blue crosses) that have Niño-3.4 peaks within 0.5 standard deviation of -0.9°C. Distinguishing the OLR La Niña years from these 8 other years using just SSTA is difficult.

In the plot described above, we selected as Niño-3.4 minima the minimum monthly averages seen around the end of the respective calendar year (from August year 0 to April year 1). This is done in order to account for the fact that not every La Niña (or El Niño) year has peak SSTAs at precisely the same time. Similar results, however, are also obtained based on fixed-time averages of Niño-3.4 values. For example, the relationship between the September–November average Niño-3.4 values and the OLNI integrated contemporaneously from 1 September to 30 November is qualitatively similar to that shown in Fig. 5b (cf. Fig. 6).

We have examined the spatial distribution of the SST and SSTAs seen in the commonly identified ENSO years (e.g., Figs. B1 and B2 in appendix B) for indication of their OLR-based categorization. We have not found a way to recover the OLR El Niño or OLR La Niña perspectives by considering just tropical Pacific SSTA conditions. ENSO-region SSTAs (e.g., Niño-3.4 or Niño-3 averages) follow rather continuous distributions (Chiodi and Harrison 2010), in which case it is more difficult to determine which and how many (if any) years deserve special attention.

The relationship between the OLR indices and ENSO SSTA behavior can be summarized as follows. The few years with the very largest amplitude Niño-3.4 SSTAs are generally among those identified by OLR, but the OLR events cannot be equivalently identified by choosing a (different) threshold value of the Niño-3.4 index. All years identified by OLR have at least moderately anomalous SSTs (e.g., Niño-3.4 amplitudes exceeding 0.85σ). Yet, several other non-OLR event years also have SSTA amplitudes in the moderate-to-strong SSTA range. Further, there is no discontinuity in the distribution of these SSTAs that corresponds to the eventlike OLR behavior.

4. Results

a. OLR anomaly composites

Composite seasonal-average OLR anomalies based on the OLR El Niño years are shown in Fig. 7. In each of the seasons considered, taken here as June through August (JJA), September through November (SON), December through February (DJF), and March through May (MAM), a broad and statistically significant

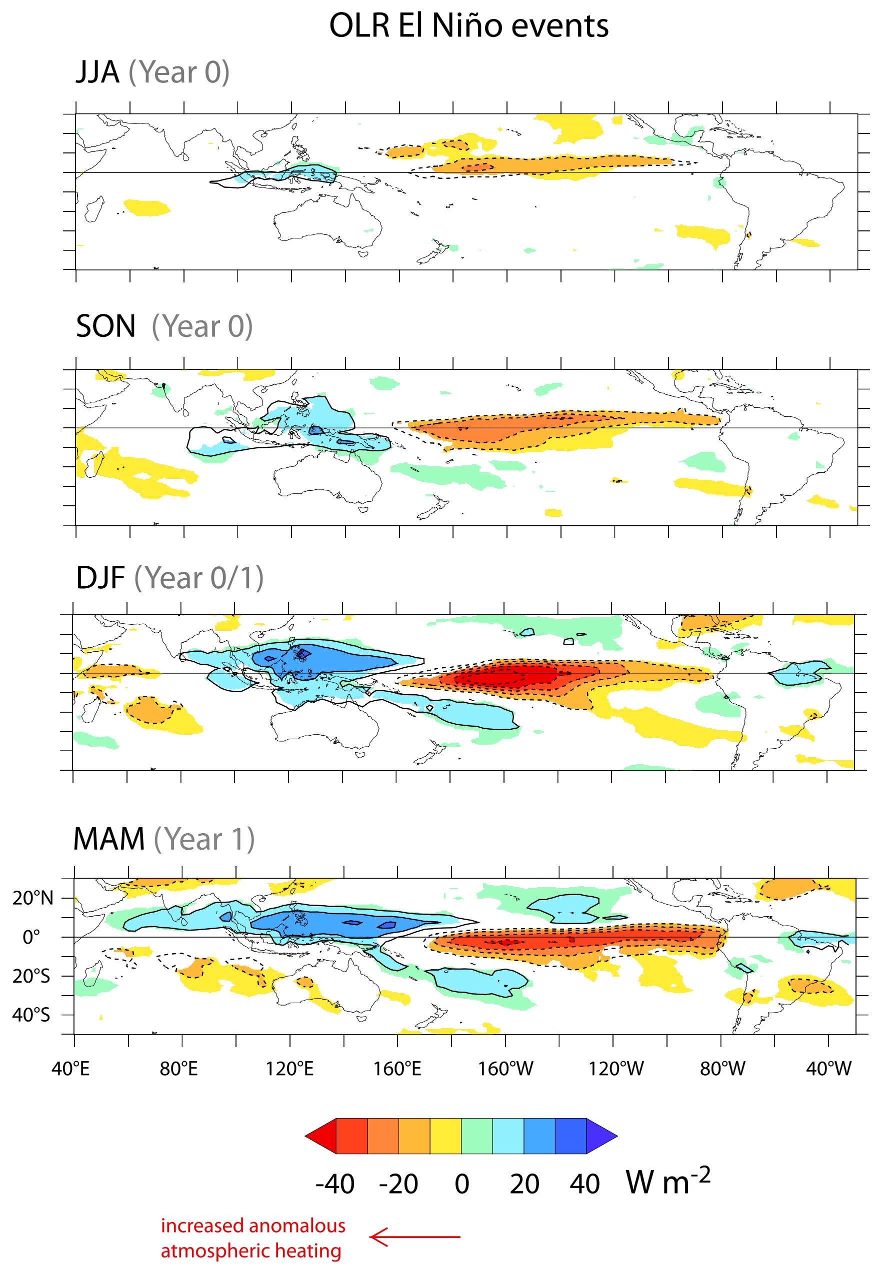

FIG. 7. OLR El Niño event composite OLR anomaly. The anomaly is shaded where amplitudes are significant at the 95% confidence level.

negative OLR anomaly (increased atmospheric heating) is seen in the central and eastern tropical Pacific from about the date line to 100°W. This anomaly feature strengthens considerably from JJA (year 0) to DJF (year 0/1) and maintains much of its amplitude through MAM (year 1). Also, a statistically significant and positive OLR anomaly is seen in the far-western Pacific that broadens and strengthens during this time. Inspection of the individual years (shown in the supplementary material) has shown that although there are some differences in OLR anomaly strength among the 4 OLR El Niño years in the earlier seasons, similar anomaly patterns with substantial strength ($>20\ \mathrm{W\,m^{-2}}$) across the tropical Pacific develop by DJF or MAM in each of these 4 years. Thus, significantly anomalous ($p > 0.95$) deep convective activity across almost the entire tropical Pacific is a robust characteristic of the OLR El Niño events.

A different type of behavior is seen in the non-OLR El Niño composite OLR anomalies. In this case, the

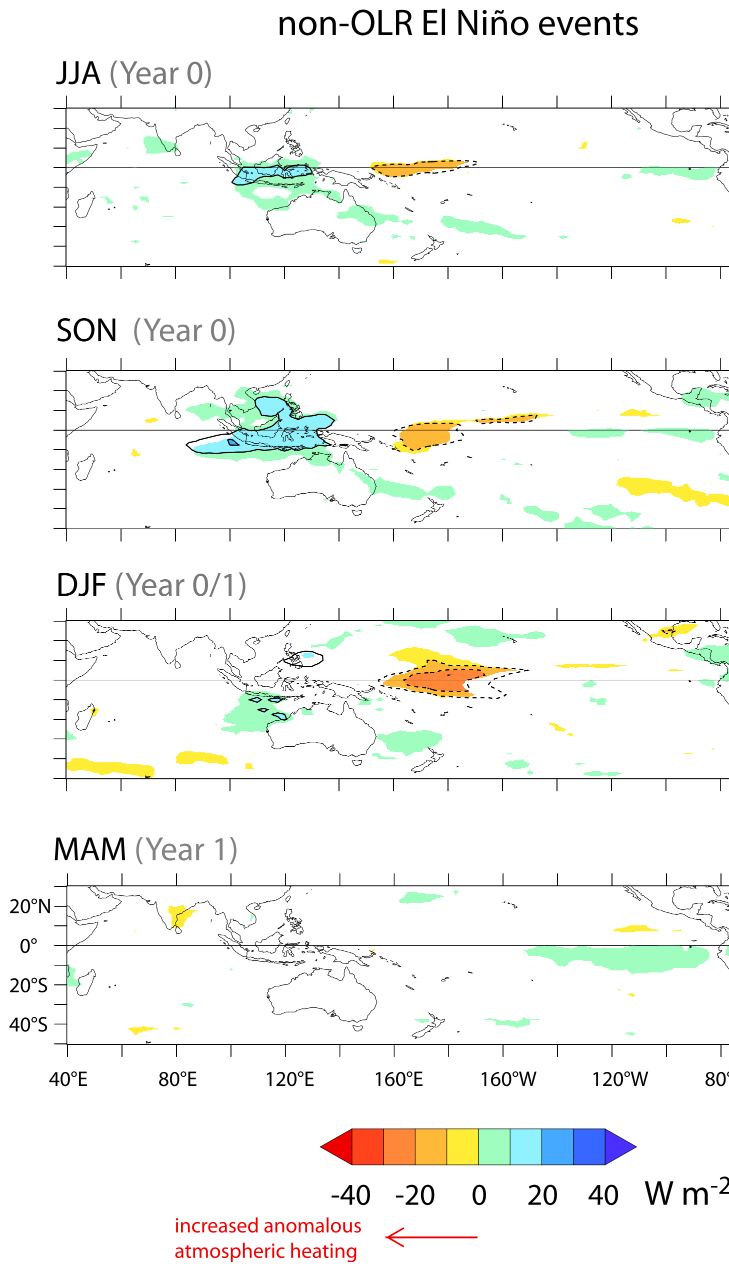

FIG. 8. Non-OLR El Niño event composite OLR anomaly. The anomaly is shaded where amplitudes are significant at the 95% confidence level.

expanse of the statistically significant and negative anomaly in the eastern central Pacific (160°–100°W) is much reduced compared with the OLR El Niño case. And although some positive and statistically significant anomaly is seen in the far-western Pacific in JJA and SON, these anomalies weaken in DJF and are no longer apparent by MAM (Fig. 8).

Like the OLR El Niño case, the OLR La Niña composite OLR anomaly patterns are statistically significant across much of the tropical Pacific (Fig. 9). Negative statistically significant anomalies are seen in this case in the far-western Pacific, whereas positive statistically significant anomalies occur in the near–date line region (roughly 150°E–150°W). Although these patterns are rough counterparts to the oppositely signed features of the OLR El Niño composites, substantial asymmetries are also apparent. Notably, in the OLR La Niña events, the positive statistically significant anomalies seen around the date line do not reach all the way to the eastern equatorial Pacific. Differences in the seasonal

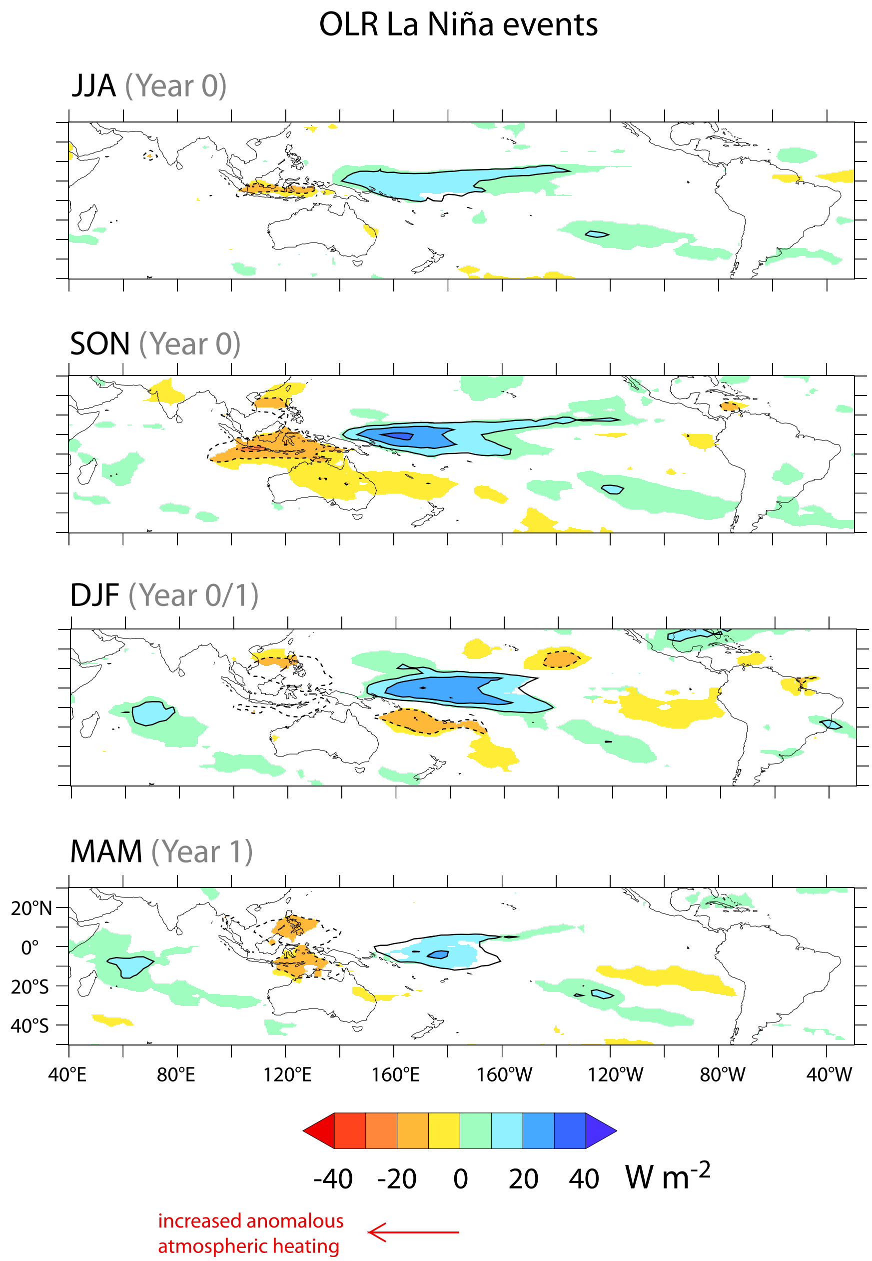

FIG. 9. OLR La Niña event composite OLR anomaly. The anomaly is shaded where amplitudes are significant at the 95% confidence level.

strength of the OLR La Niña and OLR El Niño composites are also evident. Notably, in the OLR La Niña case, the peak amplitudes are seen in SON, whereas in the OLR El Niño case, they occur in DJF.

Okumura and Deser (2010) examined composites of tropical Pacific precipitation anomaly based on El Niño and La Niña years defined using a Niño-3.4-based definition (period 1982–2008). They report that the anomaly pattern seen around the end of the calendar year (year 0/1) in the La Niña case persists longer than that seen in the El Niño case, which, according to their composites, changes character by boreal spring (i.e., MAM year 1). A different sort of progression is seen in the OLR El Niño composites shown here. In this case, the DJF (year 0/1) OLR anomaly pattern maintains amplitude and character through MAM (year 1). A very different situation, however, is seen in the non-OLR El Niño composites than in the OLR El Niño composites (including oppositely signed anomalies in the eastern Pacific in MAM). The differences in character between our and

Okumura and Deser's (2010) results likely stem from the fact that their approach mixes, in equal parts, years that are identified by us as both OLR and non-OLR El Niño years.

Examination of the OLR anomalies seen in the 6 individual OLR La Niña years (see Fig. S10 in the supplementary material) has shown that the anomaly pattern seen near the date line in SON is a robust feature of these years; each of the 6 OLR La Niña years had a coherent and substantial (20–40 $\mathrm{W\,m^{-2}}$) positive anomaly in this region in SON, whereas this feature is not seen in SON in the other years. In the subsequent DJF and MAM seasons, however, some years have anomaly amplitudes in the near–date line and far-western Pacific regions that resemble the pattern but exceed the values seen in SON, whereas others (especially 1974/75) show a different, weaker amplitude anomaly pattern. Thus, strong mature-stage (DJF and MAM) atmospheric heating anomalies appear to be a possible but not necessarily consistent feature of the OLR La Niña events, as they are defined here. On the other hand, strong and consistent forcing during both DJF and MAM was seen in each of the OLR El Niño events.

In the non-OLR La Niña case (Fig. 10), coherent and statistically significant OLR anomalies are seen only in the far-western (negative) and near–date line (positive) regions in the DJF composite. Inspection of the individual years has shown that this feature is not robust; only 3 of the 6 non-OLR La Niña years (1983/84, 1995/96, and 2000/01) have DJF anomaly amplitudes greater than 20 $\mathrm{W\,m^{-2}}$ in both the far-western and near–date line regions. In the other seasons considered, the composite non-OLR La Niña anomalies in these regions are not nearly as statistically significant as those seen in the OLR La Niña composites.

b. *Precipitation anomaly*

Precipitation composites based on the OLR El Niño, non-OLR El Niño, OLR La Niña, and non-OLR La Niña years are shown in Figs. 11–14, respectively. In this case, precipitation anomalies are shown where they reach statistical significance at the 80% confidence interval or better. Comparison with composites masked at higher levels (not shown) suggests that using an 80% cutoff in this case is useful for identifying regions with spatially coherent, if not uniformly significant, anomalies. Using a lower confidence interval obviously raises the fraction of the area that can be expected to reach statistical significance misleadingly (i.e., by chance alone). To test whether the anomaly patterns we consider are entirely dominated by such results, the global, or "field" (Livezey and Chen 1983), significance of each composite, based on the extent of the area that reaches local statistical significance, is also estimated by a Monte Carlo approach.

To understand the role of a field significance test in a study such as this, which simultaneously examines many different regions with different types of seasonal weather anomalies, it is important to recognize that some locally statistically significant anomaly should be expected even in the case that the results (composite anomaly patterns) are produced by the effects of chance alone (the "null hypothesis"). A field significance test determines, in this case, the areal-extent locally significant anomaly that must be seen in a composite in order for the null hypothesis to be disproven at the selected confidence interval.

Of the 16 (4 seasons $\times$ 4 year lists) seasonal precipitation anomaly composites shown in Figs. 11–14, only 2 are globally (60°N–60°S), or field, significant at the 95% level or better: the OLR El Niño DJF composite (shown in Fig. 11) and the OLR La Niña SON composite (shown in Fig. 13).

Many features of the anomaly patterns seen in these composites will be recognizable to readers familiar with the seminal studies of the seasonal weather anomalies associated with ENSO. For example, the locally significant anomalies seen in the SON OLR La Niña composite centered over Uruguay (dry), the islands of the far-western tropical Pacific and Australia (wet), India (wet), Sri Lanka (dry), as well as the anomalies seen in the DJF OLR El Niño composite over southern (dry) and eastern equatorial (wet) Africa, the far-western Pacific island nations and some of Australia (dry), the southern United States (wet), northeastern South America (dry), and southern Brazil and Uruguay (wet) are all consistent, at least in a broad sense, with anomalies previously highlighted by the work of Ropelewski and Halpert (1987, 1989), who examined an earlier period than is considered here. [There is only 1 year of overlap among the 19 La Niña and 25 El Niño years composited by Ropelewski and Halpert (1987, 1989) and those considered here.] These particular features can be seen in closer detail than is shown in Figs. 11 and 12 and in comparison to their non-OLR event counterparts in Figs. 15 and 16 (SON La Niña and DJF El Niño, respectively).

Many of these regional anomalies remain statistically significant in the subsequent seasons (i.e., MAM in the OLR El Niño case and DJF in the La Niña case), which yield precipitation composites that remain globally significant at the 90% level. Such features include the anomalies seen over northeastern South America and Uruguay in the MAM OLR El Niño case. Inspection of the individual years (shown in supplementary material)

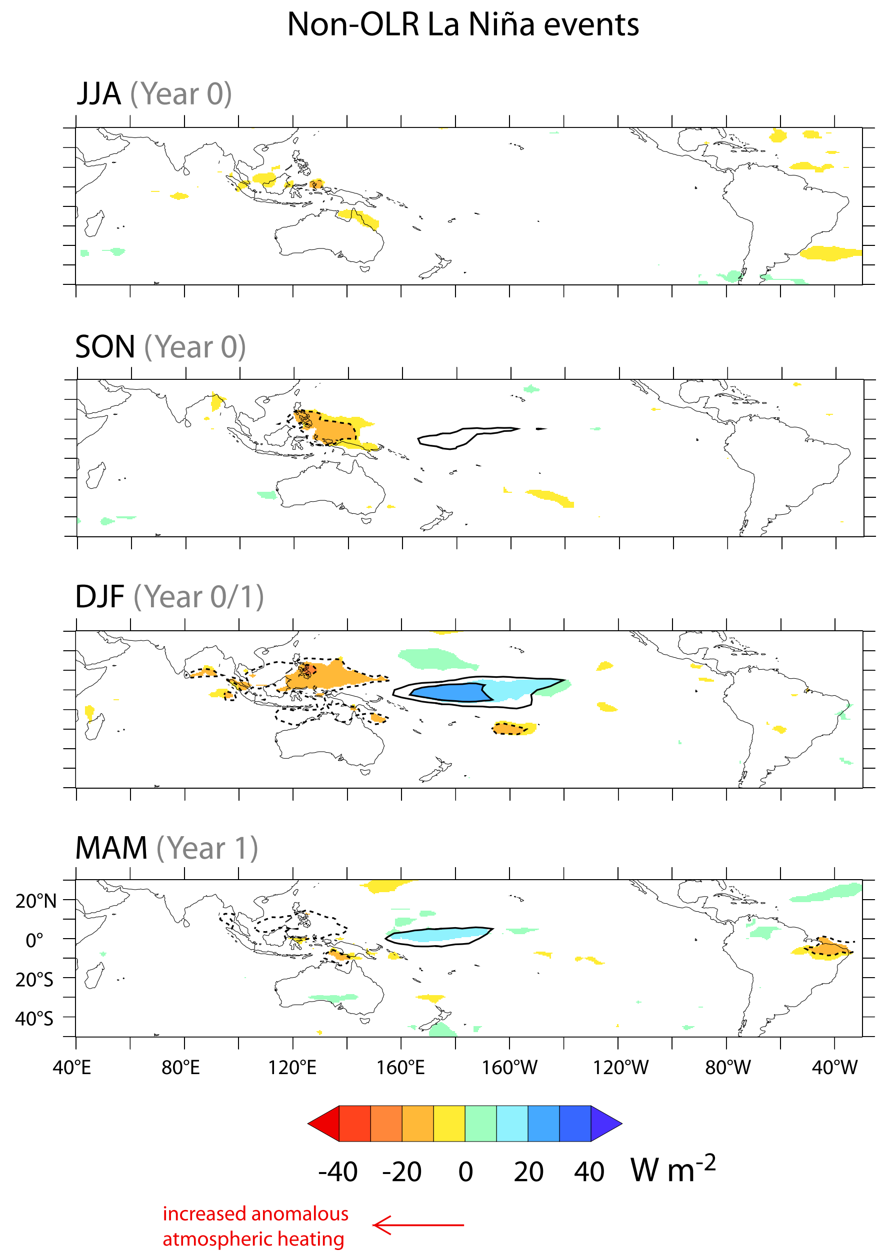

FIG. 10. Non-OLR La Niña event composite OLR anomaly. The anomaly is shaded where amplitudes are significant at the 95% confidence level.

reveals that these features are among the most consistent highlighted by these results. The generally high level of consistency between the composites discussed here and previously by Ropelewski and Halpert (1987, 1989) suggests that they may be stable features of the influence of ENSO on seasonal weather anomalies.

Other significant anomalies seen in these OLR-identified composites, such as the dry (wet) anomalies seen in SON over the Horn of Africa and Saudi Arabia in the OLR La Niña (El Niño) composite and the wet anomalies seen over southwestern China in the DJF and MAM OLR El Niño composites (perhaps also the dry anomaly over Thailand in this latter case), were not as prominent in the earlier studies (Ropelewski and Halpert 1987, 1989; Kiladis and Diaz 1989). And in some instances, statistically significant anomalies are not seen in the OLR-identified composites when and where they may have been expected based just on the seminal studies (e.g., very little statistically significant anomaly is seen over India in the JJA OLR El Niño

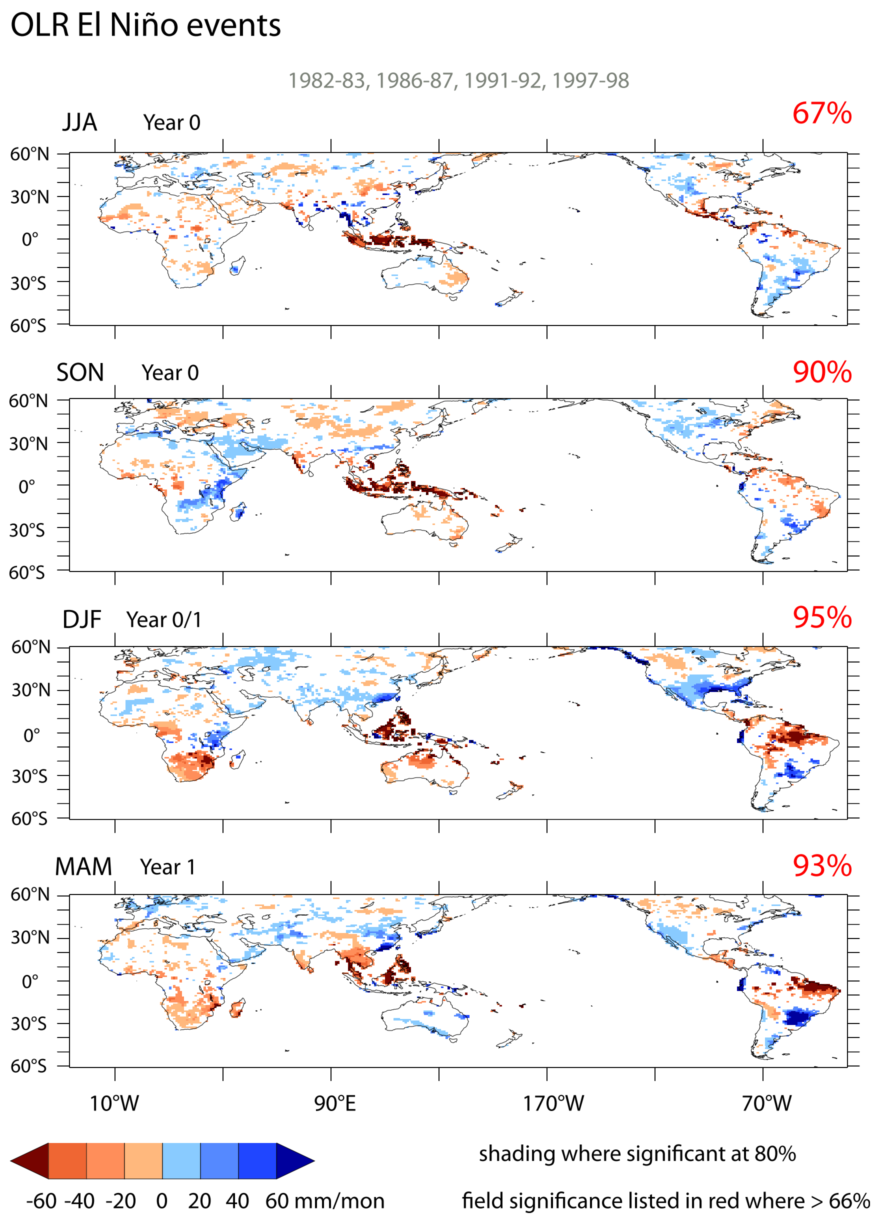

FIG. 11. OLR El Niño event composite precipitation anomaly. Shading where amplitudes are significant locally at the 80% confidence level. Field significance listed in red.

composite). These differences may be the result of seasonal impacts now better revealed by recent improvements in the observing system, changes in the influence of ENSO, or artifacts of the particular years chosen in this case.

A different type of anomaly pattern is seen in the precipitation composites based on the non-OLR El Niño and non-OLR La Niña years (Figs. 12 and 14). For example, in SON, when the OLR La Niña case was found to reach peak global significance, there are very few areas in the non-OLR La Niña composite that yield locally significant anomalies, and those that do are characterized by a relatively regionally incoherent mix of positive and negative anomalies. In DJF, when the OLR El Niño case reached peak global significance, the non-OLR El Niño composite does not yield enough locally significant anomaly to reach global significance at even the 50% confidence level (it contains less locally statistically significant anomaly than should be expected based on the effects of randomness alone). With the exception of South America, which in the DJF (but not MAM) non-OLR El Niño case resembles a weaker amplitude version of that seen in the OLR El

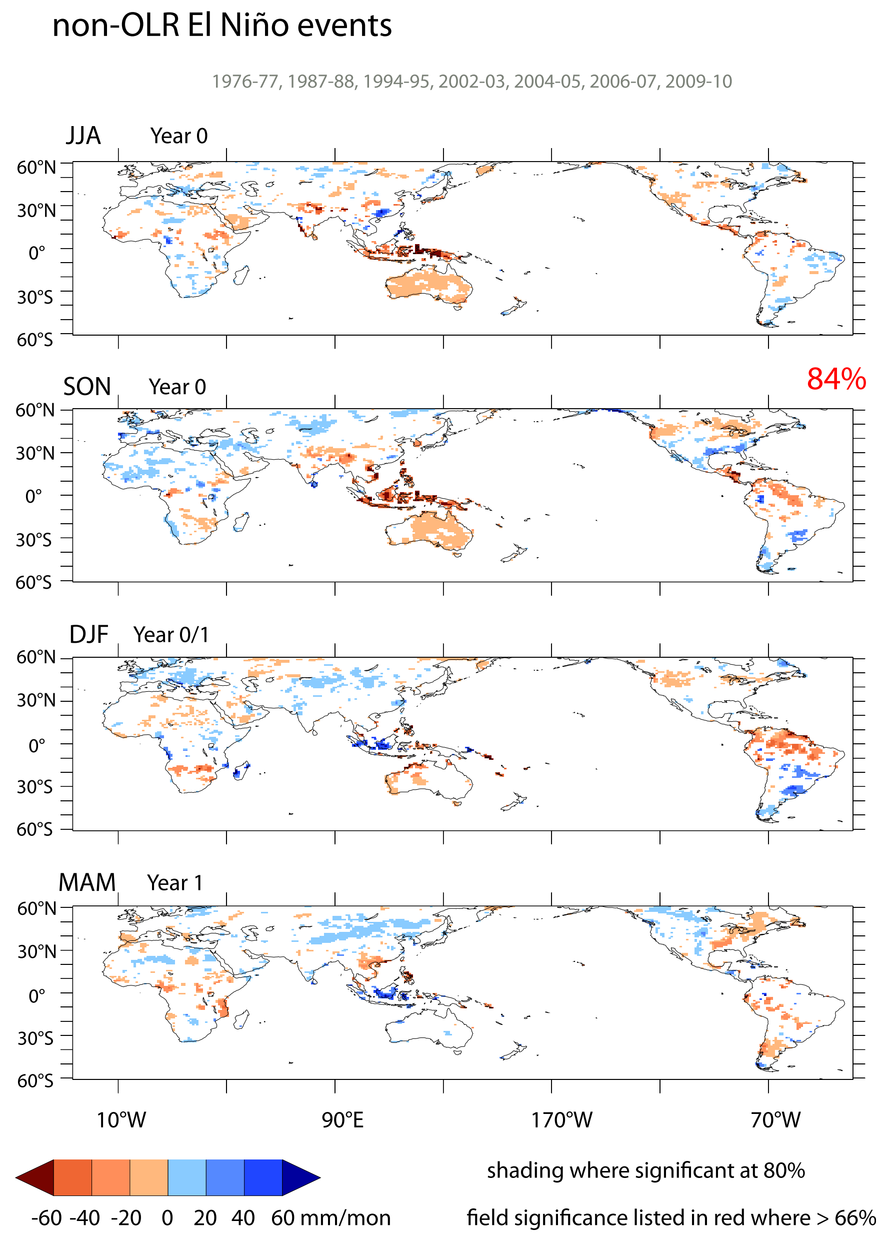

FIG. 12. The non-OLR El Niño event composite precipitation anomaly. Shading where amplitudes are significant locally at the 80% confidence level. Field significance listed in red.

Niño composite, it is difficult to find regions that are statistically significant and have the same sign in both the DJF OLR and non-OLR El Niño composites.

Based on the Monte Carlo methods used here, none of the non-OLR ENSO composites reach field significance at the 90% confidence level. It should be noted, however, that the SON non-OLR El Niño composite is close to being field significant at 90% ($p = 0.84$) and has a coherent and statistically significant dry anomaly over most of Australia that may be deserving of further consideration. Interestingly, dry anomaly over most of Australia can also be seen in the preceding JJA non-OLR El Niño composite, and inspection of the individual years (see supplementary material) reveals that dry anomalies with amplitudes and patterns like those seen in the composites are a relatively consistent (e.g., 5 out of 6) feature of these years, in these seasons. At least over some regions of Australia [e.g., south and southwest of Australia in the work of Ropelewski and Halpert (1987, 1989); see also the SON results of Kiladis and Diaz (1989)], June–November year 0 El Niño effects on Australian rainfall have also been found

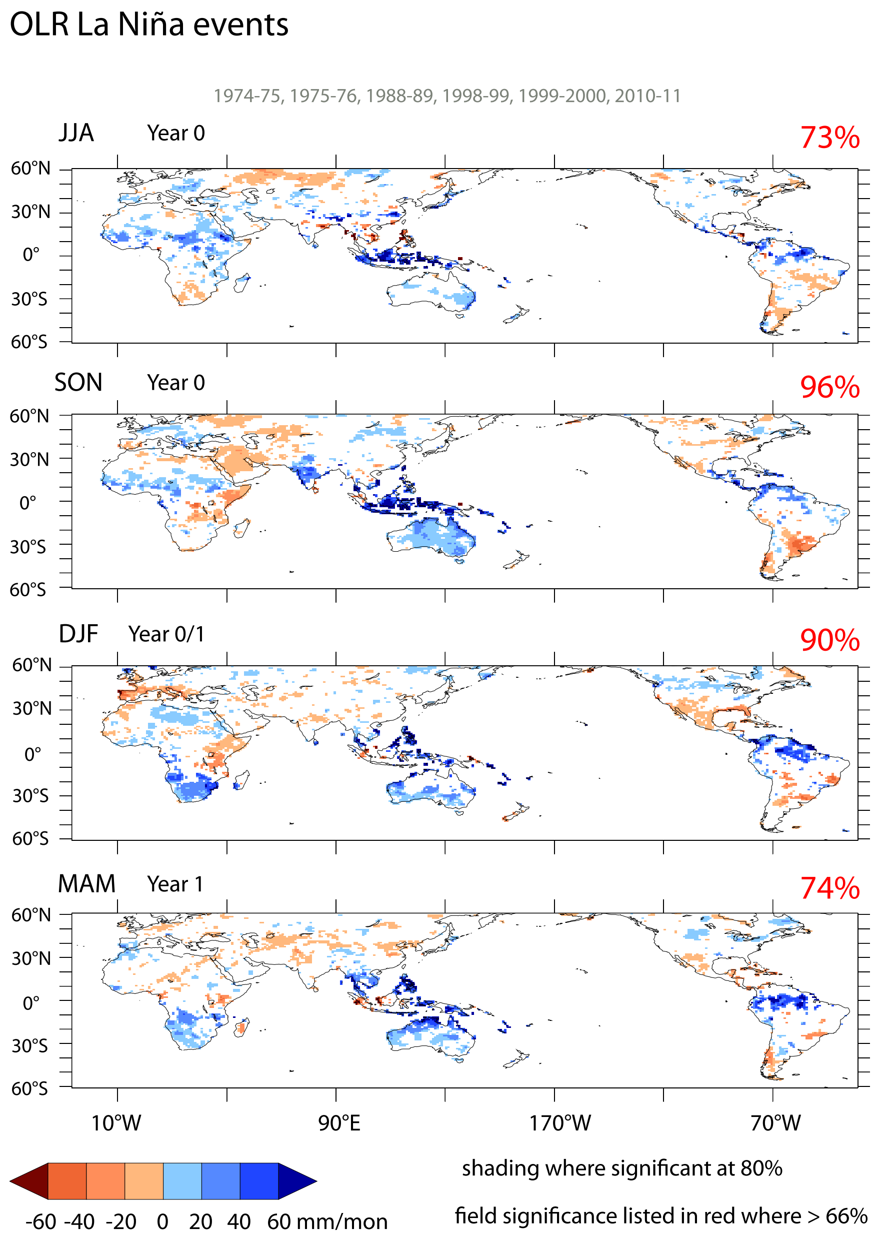

FIG. 13. The OLR La Niña event composite precipitation anomaly. Shading where amplitudes are significant locally at the 80% confidence level. Field significance listed in red.

previously. That more locally statistically significant dry anomaly is seen over Australia in the non-OLR El Niño than OLR El Niño composite raises the possibility that the anomalous atmospheric heating conditions associated with the non-OLR El Niño years may be more conducive to dryness over Australia than the conditions associated with the OLR El Niño years. In the non-OLR El Niño case, event onset stage (boreal summer–autumn) convection is substantially reduced over the far-western Pacific and eastern tropical Indian Ocean but does not increase over the central and eastern tropical Pacific nearly to the extent seen in the OLR El Niño years. Diagnostic modeling, likely with coupled ocean–atmosphere models, which is beyond the scope of this study, will be needed to more fully explore the mechanisms linking these two different types of OLR behavior and rainfall anomalies over Australia.

We are aware that some studies have called attention to event-to-event differences in the locations (e.g., central versus eastern tropical Pacific) of the maximum El Niño SSTAs [see Capotondi et al. (2015) for a review]. There is, however, no simple relationship between this

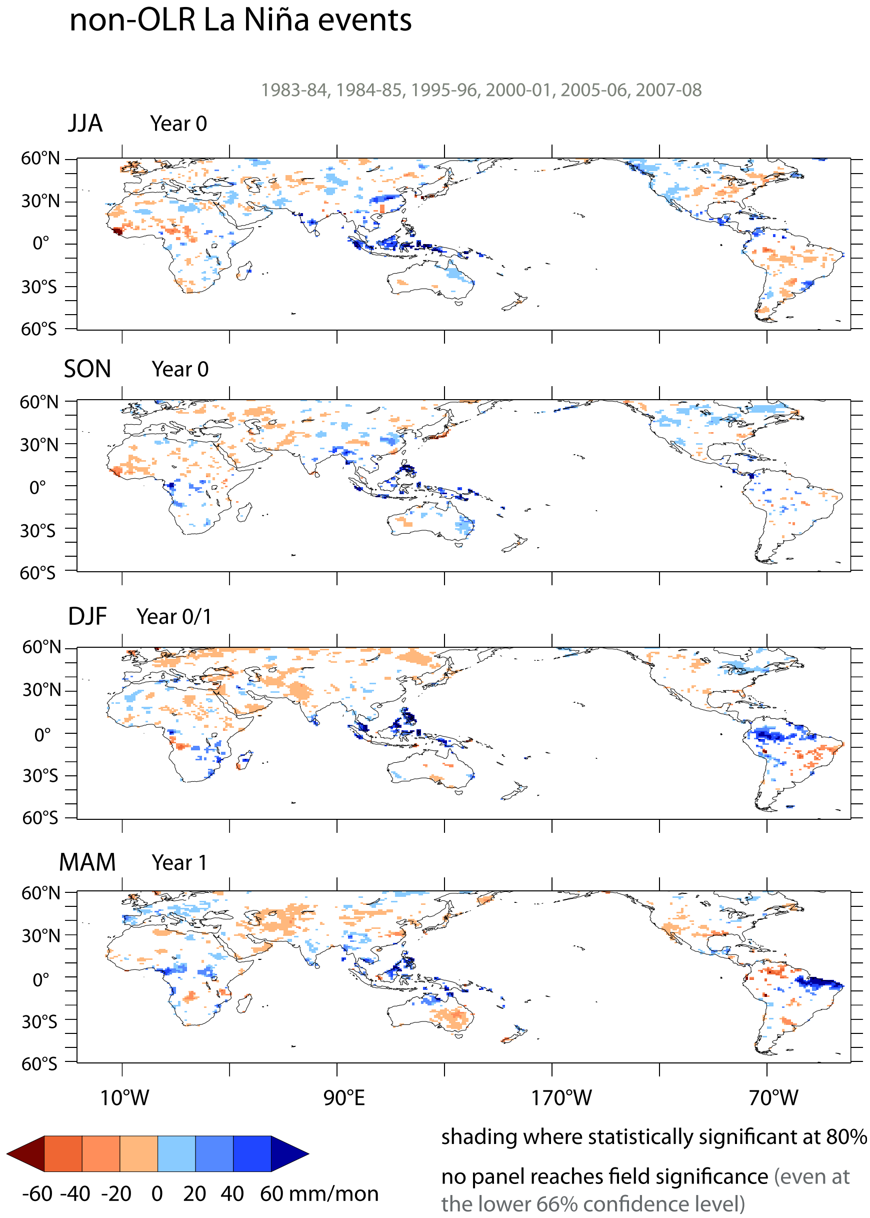

FIG. 14. The non-OLR La Niña event composite precipitation anomaly. Shading where amplitudes are significant locally at the 80% confidence level. Field significance listed in red.

aspect of SSTA and OLR behavior (as was discussed by Chiodi and Harrison 2013). For reference and comparison purposes, we have computed the DJF precipitation anomaly composites based on the non-OLR El Niño years that are identified alternatively as El Niño Modoki, warm pool (WP) El Niño, or central Pacific (CP) El Niño years, by Ashok et al. (2007), Kug et al. (2009), and Yu et al. (2012), respectively. We find that the patterns seen in these Modoki/WP/CP El Niño composites are easily reproducible, based on chance alone, in terms of the amounts of statistically significant anomaly seen in them (composites shown in Fig. C1). It appears that the dominant (boreal) wintertime precipitation pattern associated with El Niño is basically that discussed previously by Ropelewski and Halpert (1986) and seen rather robustly over recent decades during the OLR El Niño events.

5. Nonlinear aspects of the precipitation composites

Some studies (e.g., Kumar et al. 2007) have suggested, based partly on atmospheric general circulation model experiments, that the influence of ENSO on global

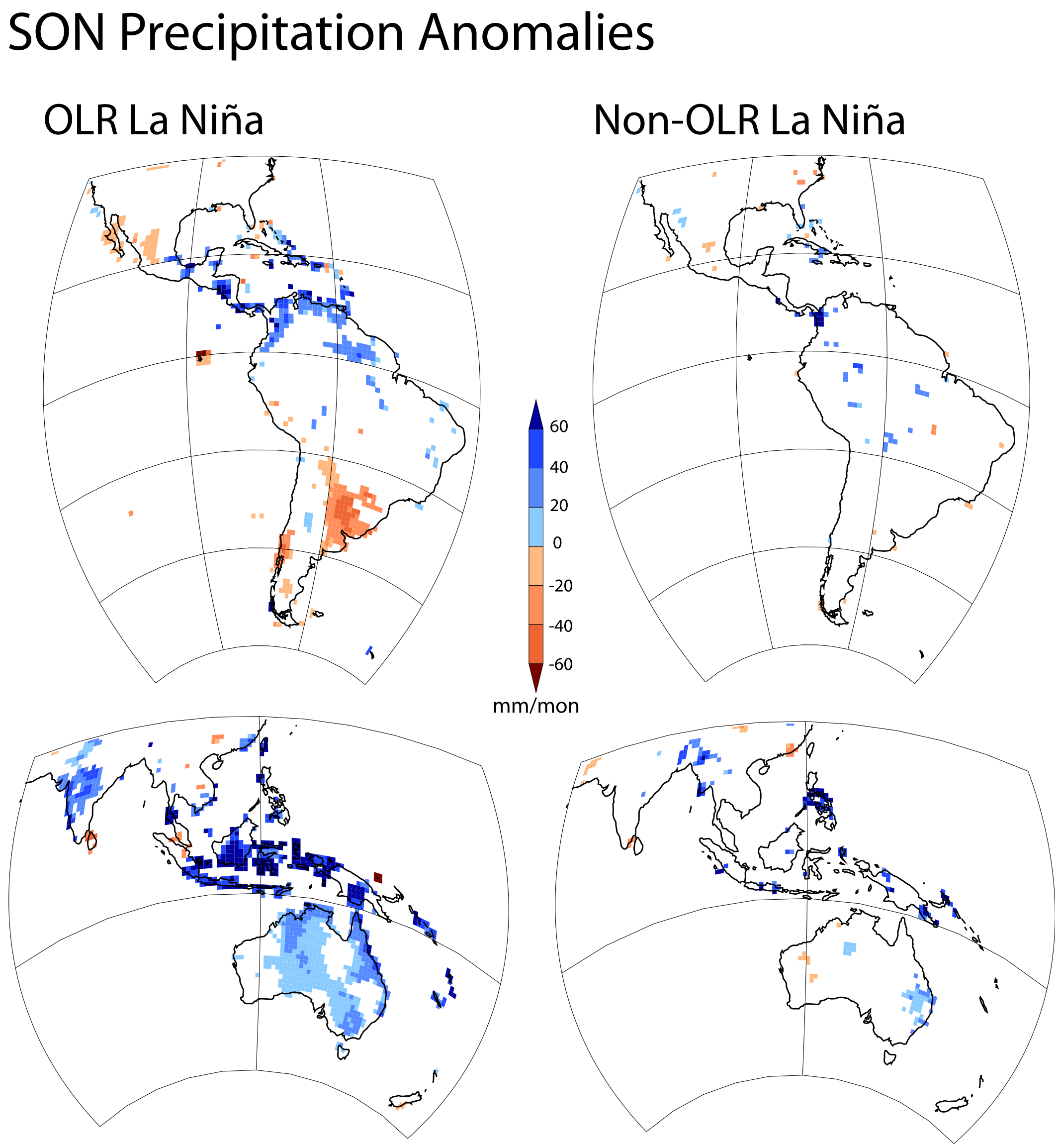

FIG. 15. Regional perspective SON-average precipitation anomaly composites based on the (left) OLR La Niña and (right) non-OLR La Niña years. The precipitation anomaly is shaded in this case where significant at the 90% confidence interval.

atmospheric variability is well represented by a statistical model that predicts atmospheric anomalies based on a linear regression with Niño-3.4 SSTA (i.e., the relationship between Niño-3.4 SSTA and atmospheric response is quasi linear). Our results suggest otherwise, with the OLR events having substantial and robust precipitation anomaly patterns and the non-OLR events being largely indistinguishable from randomness. In the review process, the issue arose of whether a quasi-linear model (one that posits a linear relationship between Niño-3.4 and atmospheric response to ENSO but also accounts for noise, or sources of atmospheric variability unrelated to ENSO) could be considered consistent with our precipitation composite results. The argument in favor of this is that the OLR-identified El Niño and La Niña years have, on average, stronger ENSO SSTA amplitudes than the other non-OLR years. We have examined this question using Monte Carlo methods that simulate land precipitation anomaly in the strongly affected DJF season according to a quasi-linear model based on the ‘‘signal-to-noise’’ measure used by Kumar et al. (2007), who also considered DJF.

The Northern Hemisphere winter (e.g., DJF) is the time of year during which ENSO events typically peak in the tropical Pacific. It is also when many of the statistical linkages between ENSO-state and seasonal weather

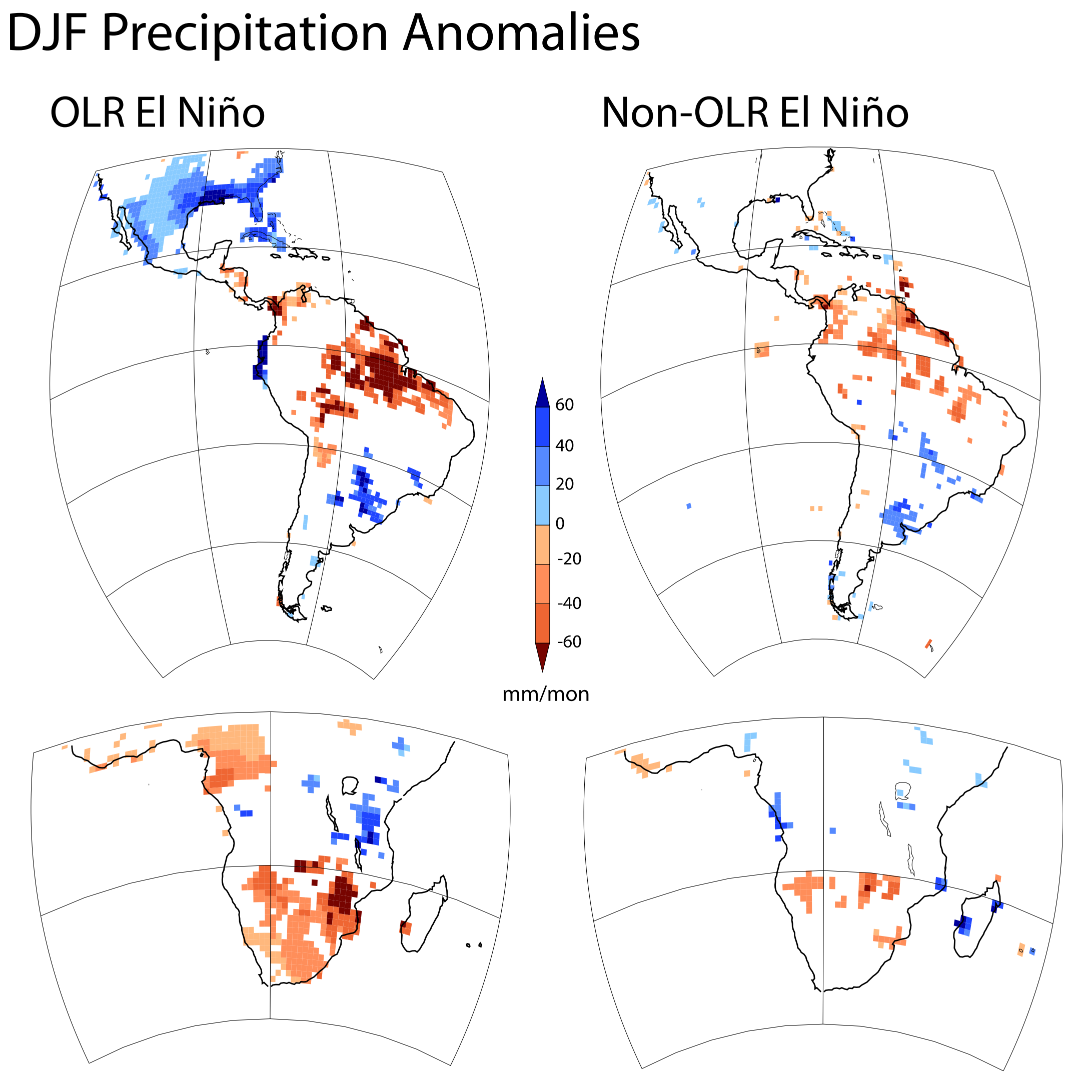

FIG. 16. Regional perspective DJF-average precipitation anomaly composites based on the (left) OLR El Niño and (right) non-OLR El Niño years. The precipitation anomaly is shaded in this case where significant at the 90% confidence interval.

anomalies elsewhere are at, or near, their strongest. The global land precipitation composites based on the OLR-identified subsets of El Niño and La Niña years each reach field significance during DJF based on the amount of locally statistically significant anomaly contained in them (at the 90% and 95% levels, respectively). By the same measure, however, the non-OLR El Niño and non-OLR La Niña precipitation composites are indistinguishable from randomness at this time (they contain amounts of locally statistically significant anomaly that rank at the 41st and 47th percentile, respectively—i.e., slightly less than the amount expected based on pure random selection, which is 50%).

To test whether these observational results are consistent with the quasi-linear model, we follow the methods of Kumar et al. (2007) in computing a signal-to-noise ratio based on a linear regression between DJF-averaged precipitation anomaly and DJF-averaged Niño-3.4 SSTA. In this case, the ‘‘signal’’ is the amount of observed precipitation variability that is linearly related to the Niño-3.4 index, and the ‘‘noise’’ is the remainder. These terms are determined at each land location by calculating the regression coefficient c in the following linear model:

$$p'(t) = c\mathrm{NI\tilde{N}O3.4}(t) + n(t). \qquad (1)$$

Here $p'(t)$ is the precipitation anomaly averaged over DJF of year t, and c is defined at each land location based on least squares methods. The signal-to-noise ratio, then, is the standard deviation of the $c\tilde{N}IÑO3.4(t)$ term computed over the 37 DJFs in the study period divided by the standard deviation of $n(t)$ over that same time.

The DJF precipitation anomaly signal-to-noise ratio thus defined is shown in appendix D, for reference (Fig. D1). Comparison with the precipitation composites shown in Figs. 11 and 13 reveals that the strongest signal-to-noise ratios are found mainly in the same regions that have statistically significant anomalies in the OLR El Niño and OLR La Niña composites.

We use Monte Carlo methods to test whether this linear model is consistent with the observed variability. Specifically, we examine whether the model can easily reproduce precipitation composites that in one case (based on the OLR-identified subset of years) reach field significance at standard confidence intervals, while the others (based on the non-OLR subset of years) are indistinguishable from randomness.

To proceed, we need to decide how many land locations should be resolved in the simulation. Since the precipitation time series at each grid point in a dataset like the one we consider should not generally be considered to vary independently from those surrounding it, a first step here involves estimating the effective number of spatial degrees of freedom (ESDOF) contained in the GPCC land precipitation data. We have done this based on the methods of Bretherton et al. (1999), as described in appendix D, and found that a range, rather than a specific number, of ESDOF is suggested by this approach. We have therefore repeated the simulation over an extended range of ESDOF (25–200).

To simulate the land precipitation anomaly, the cNIÑO3.4(t) time series is specified as the signal at each land location. The signal stays fixed during the simulation. A different independently selected noise term, which we select from a random normal distribution with standard deviation chosen to match the ratio shown in Fig. D1, is then added to the signal in each iteration. We have confirmed that the observed noise terms do not generally violate the classic Kolmogorov–Smirnov test for normality, suggesting that the use of a random normal distribution is appropriate in this case. The simulated data are then tested for field significance (after each iteration) following the same procedure used for the observations.

We find that the simulation's quantitative behavior depends on the ESDOF used, but even in the most lenient scenario (lowest ESDOF), it is at least "unlikely" (Mastrandrea et al. 2010) that the quasi-linear model yields a non-OLR La Niña (El Niño) global land precipitation anomaly composite that contains as little, or less, statistically significant anomaly as is seen in the observations (see Table 2). In other words, the linear model usually predicts that a stronger response (more statistically significant anomaly) should be seen in the non-OLR composites than is actually observed. And if the initial estimates of ESDOF are conservative, as we expect, then it is at least "very unlikely," and quite possibly "exceptionally unlikely," that the quasi-linear model is consistent with the observed variability in this respect. Under these assumptions, the linear model almost always predicts that the non-OLR precipitation composites would also be at least moderately field significant (in addition to the OLR event composites).

TABLE 2. Chance that the Monte Carlo simulation (based on linear regression with Niño-3.4 index) reproduces a non-OLR ENSO year precipitation composite with as little, or less, statistically significant anomaly as is seen in the observations.

ESDOF	25	50	75	100	125	200
Non-OLR La Niña	19%	12%	9%	6%	4%	0.2%
Non-OLR El Niño	18%	14%	10%	6%	5%	0.3%

The results of this section can be summarized as follows. Depending on the ESDOF assumed, it is unlikely to exceptionally unlikely that the quasi-linear relationship of Kumar et al. (2007) can explain our composite results, which find strong and robust precipitation anomaly patterns in the DJF OLR El Niño and OLR La Niña composites but composites that are indistinguishable from noise based on the other non-OLR ENSO years. In other words, the differences between the OLR-event and non-OLR precipitation composites cannot easily be anticipated by looking at their respective Niño-3.4 behavior. The Niño-3.4-based quasi-linear model fails because, given the strength and consistency of the precipitation anomaly patterns in the OLR-identified events, the quasi-linear model predicts that more statistically significant anomaly should be seen in the other years (non-OLR years) than is actually seen in the observations.

These results support our conclusion that it is useful to pay attention to OLR for the purposes of identifying the years that are most likely to exhibit the seasonal weather anomaly patterns that have traditionally been associated with El Niño and La Niña extremes.

6. OLR- and SSTA-based outlooks on ENSO

The OLR indices discussed above are able to identify the tropical Pacific anomaly states most likely to have a meaningful (significant amplitude) and consistent influence on global seasonal weather anomalies. The OLR El Niño and OLR La Niña years are typically identified by the end of boreal autumn, making their later-season composites directly useful to seasonal forecasting efforts in the ensuing winter and spring seasons, even without the ability to predict OLR.

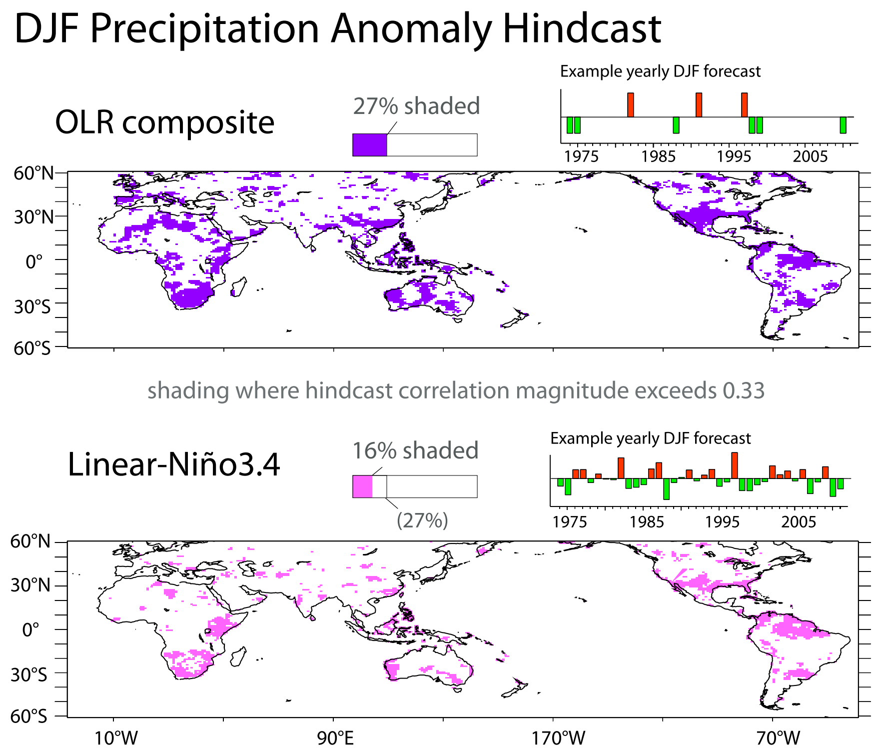

FIG. 17. DJF precipitation anomaly hindcast results for the period 1974–2011. (top) Shading is where OLR-hindcast anomaly correlation magnitude exceeds 0.33, and 27% of the land is shaded. In the OLR hindcast, finite (nonzero) anomalies are specified in the hindcast only in the 9 years identified by the OLR indices prior to boreal winter. The anomaly correlation, however, is computed over all years. (bottom) Shading is where the linear-regression hindcast anomaly correlation magnitude exceeds 0.33. In this case, only 16% of the land is shaded, even though finite anomalies are specified in each year.

In review, we were asked if consideration of tropical Pacific OLR behavior can be expected to increase measures of forecast skill computed over all years, not just the subset identified by OLR. To examine this, we have conducted a retrospective forecast (hindcast) experiment in which global precipitation anomaly in the strongly affected DJF season (1974–2011) is hindcast based on information available by the beginning of December year 0. We consider two approaches for comparison purposes: one based on the OLR indices and their associated precipitation composites and the other based on Niño-3.4 SSTA and its linear regression with global precipitation.

In the linear regression case, we hindcast year 0/1 DJF precipitation anomaly based on its linear regression with year 0 SON averages of the Niño-3.4 index. We use SON averages because they are available by the beginning of December to forecast DJF conditions. Based on the null hypothesis of random correlation with a Gaussian time series, the hindcast anomaly correlation computed over the 37 seasons considered reaches statistical significance at the 95% confidence level when its absolute value exceeds 0.33 (Fisher's z method). The linear-regression hindcast anomaly correlation exceeds this level over 16% of the land between 60°S and 60°N (Fig. 17, bottom panel).

In the OLR-based hindcast, we apply the OLR El Niño and OLR La Niña composites in the years that are identified by the OLR El Niño and OLR La Niña indices by the end of autumn (again using tropical Pacific information available by boreal autumn to predict wintertime global precipitation conditions). Hence, the OLR El Niño composite is applied in the 3 years identified by the OLR El Niño index by the beginning of December year 0 (1 of the 4 OLR El Niño years is left out because it was not identified until after that date), and the OLR La Niña composite is applied in all 6 OLR La Niña years, because all 6 of them are distinguished by OLR behavior by December. This gives us 3 + 6 = 9 years in which a nonzero precipitation anomaly is specified. Thus, most years are predicted to have zero precipitation anomaly in this case. We nonetheless compute the anomaly correlation coefficient between the OLR hindcast and the observed DJF precipitation anomaly over all 37 years.

The OLR-case hindcast anomaly correlation reaches the 0.33 level over 27% of the land between 60°S and 60°N (Fig. 17, top panel). This is almost twice the amount that reaches this level in the linear regression case. Most (75%) of the land area that reaches this level in the linear regression case is contained within the regions that do so in the OLR case. In the majority of these regions, the stronger correlation is produced by the OLR hindcast, which produces a spatially averaged anomaly correlation of 0.43 over the regions shaded in the top panel of Fig. 17. In the OLR case, the strongest correlations are reached mainly over the same regions that have statistically significant OLR El Niño and OLR La Niña composite precipitation anomalies (cf. Figs. 11, 13, and 17). A useful amount of variance is captured by this hindcast in these regions.

We have confirmed that if the ''leave one out'' method is employed, in which case the year being predicted is left out of the regression/composite, then the fraction of land area that reaches correlation amplitudes of 0.33 or better is reduced in each case, but proportionately so that the OLR hindcast continues to reach this level over more area than the linear-regression hindcast.

This hindcast examination assumes a prior knowledge of the OLR-event composites in one case and the Niño-3.4 linear-regression coefficients in the other. We offer it not as a specific forecasting strategy but to illustrate that in most of the affected areas, the OLR hindcast performs as well as, or better than, the more commonly used linear-regression approach, even though no ENSO-type prediction is made in most of the years based on OLR.

We have also examined what happens if the composite approach is alternatively repeated by keeping the number of El Niño and La Niña event years fixed but selecting them based on the highest/lowest SON-average Niño-3.4 values (rather than OLR indices). This amounts to replacing 2 OLR El Niño years (1986/87 and 1991/92) and 1 OLR La Niña year (1974/75) with other years. In this case, 21% of the land area reaches a correlation of 0.33 or better, which is more area than the linear regression case but still less than the original OLR-composite case. This result is consistent with the view that the OLR El Niño and OLR La Niña years are among those with the strongest SSTAs but cannot be equivalently identified by raising the threshold on the Niño-3.4 index. Also, it is notable that there is no discontinuity in the SSTA distribution that suggests using these numbers of El Niño and La Niña years (as there is for the OLR-based indices).

In summary, a forecast strategy that employs the OLR perspective on the relationship between ENSO and seasonal precipitation anomalies remains deserving of attention. In this perspective, greater confidence can be placed in predicting ENSO-associated anomalies in the handful of OLR-identified years, whereas identifying predictive skill from other sources of variability (i.e., something other than the anomaly state of the tropical Pacific) is key in the other years.

7. Summary and discussion

It is well known that there is generally large event-to-event variability in seasonal precipitation anomaly patterns associated with El Niño and La Niña events defined by their Niño-3.4 values and the common definition thresholds. We have shown here that taking an OLR perspective to identify El Niño and La Niña events based on their characteristic OLR features offers a way to clearly identify subsets of years with highly statistically significant regional precipitation anomaly patterns and that many of these patterns are quite robust from year to year. Evidently, the tropical Pacific anomaly conditions present in OLR event years, which we call OLR El Niño and OLR La Niña events, are strongly connected to the processes that control global seasonal precipitation anomalies.

The OLR event years are distinguished by OLR-index values that attain a rather clear separation (>0.5 standard deviation) from the background variability seen at other times, including other non-OLR ENSO years. There is no simple way to recover the OLR-event perspective by looking at ENSO SSTA; raising the threshold on the common Niño-3.4-based definitions does not yield the same list of years (some of the years with the strongest ENSO SSTAs are not among those identified as OLR events), and there is no comparable separation in Niño-3.4 SSTA, which follows a rather continuous distribution. The OLR El Niño and OLR La Niña events stand out based on OLR, but only the largest stand out based on SSTA.

To identify the OLR events, we have made use of indices constructed from OLR observations, which have been available from the mid-1970s. We have used the OLR El Niño index of Chiodi and Harrison (2013), which is based on monthly average conditions over the eastern central equatorial Pacific and usefully identifies when deep convection has moved farther eastward into the cold tongue than normal. To identify the OLR La Niña events, we have introduced a new index that counts the number of nearly clear-sky days in the heart of the normal region of deep equatorial atmospheric convection. This index is motivated by the fact that easterly wind surges, which are associated with reduced deep atmospheric convective activity in the region, are

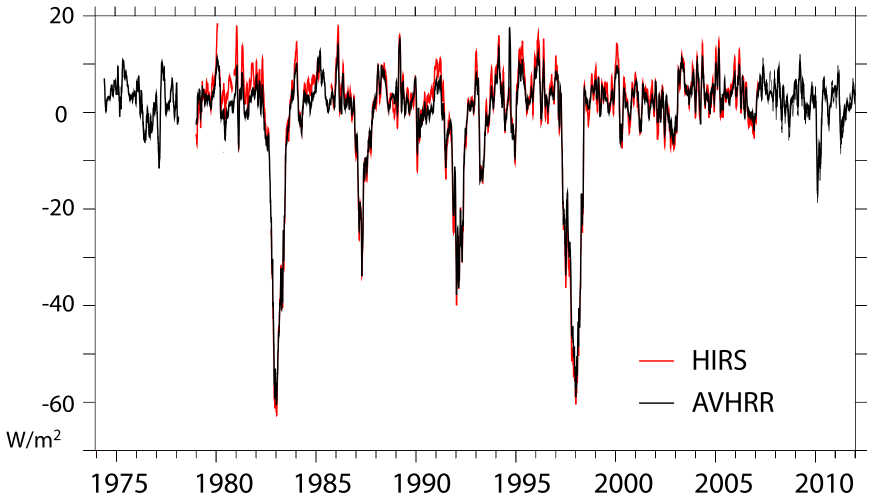

FIG. A1. The OLR El Niño index calculated based on HIRS (red curve; NOAA OLR climate dataset) and AVHRR (black curve; NOAA interpolated) based OLR data.

fundamental to the onset and maintenance of La Niña SSTA conditions (Chiodi and Harrison 2015). We present seasonal precipitation anomaly composites, masked for statistical significance over the 4 OLR El Niño years and separately over the 6 OLR La Niña years. Further, we show how similar the patterns are among the individual years within each composite (see supplementary material). These results extend the work of Chiodi and Harrison (2013), which considered El Niño–related seasonal weather anomalies over the contiguous United States, to global seasonal precipitation anomalies.

Precipitation anomalies that are globally (or field) significant at the 90% confidence interval (or better) are identified in the wintertime (DJF year 0/1) OLR La Niña composite, as well as in the wintertime OLR El Niño composite. All 6 years in the OLR La Niña composite as well as 3 of the 4 years in the OLR El Niño composite are identified by the respective OLR indices in time to be of use to wintertime and later seasonal forecasting efforts. To the extent the behavior seen in the study period continues, these indices will provide a useful indicator for the impacts of these events on wintertime precipitation anomaly, even without longer lead forecasts of tropical Pacific OLR behavior.

Globally significant precipitation anomaly is seen at the 90% level in the spring (MAM year 1) OLR El Niño composite as well. The OLR El Niño index, therefore, also does not require longer-lead forecasts of OLR in order to be a useful indicator for the impacts of OLR El Niño events on springtime precipitation.

Globally significant precipitation anomaly is also seen at the 90% level or greater in the autumn (SON year 0) OLR La Niña and OLR El Niño composites. The OLR La Niña and OLR El Niño indices, therefore, would require longer-lead forecasts of OLR in order to be useful indicators for the impacts of OLR La Niña and OLR El Niño events on autumn precipitation. The prospects for doing this deserve further study.

In addition to the OLR-identified years, the NOAA historical ENSO definition, based on 5 consecutive months of the 3-month running average Niño-3.4 SSTA $>0.5°$ or $<-0.5°C$, gives ENSO status to several others in the study period that are not identified based on OLR. Although consistent precipitation anomaly patterns are seen in the far-western Pacific and over Australia in the JJA and SON non-OLR El Niño composites (suggesting this area as one in need of further study for regional mechanistic understanding and forecast effectiveness), our results do not support widespread influence of these non-OLR ENSO years on global precipitation anomaly patterns. In most areas, the non-OLR years, on average, do not exhibit statistically useful precipitation anomaly patterns.

Based on the Monte Carlo method used, none of the non-OLR precipitation composites reach field significance at the 90% level or better. Notably, in contrast to both the DJF OLR El Niño and DJF OLR La Niña cases, the non-OLR DJF composites even fail to show the amounts of locally statistically significant precipitation anomaly that should be expected based on the effects of chance (random selection of years) alone. This difference between the OLR and non-OLR global precipitation composites is not consistent with the assumption that a linear relationship exists between global

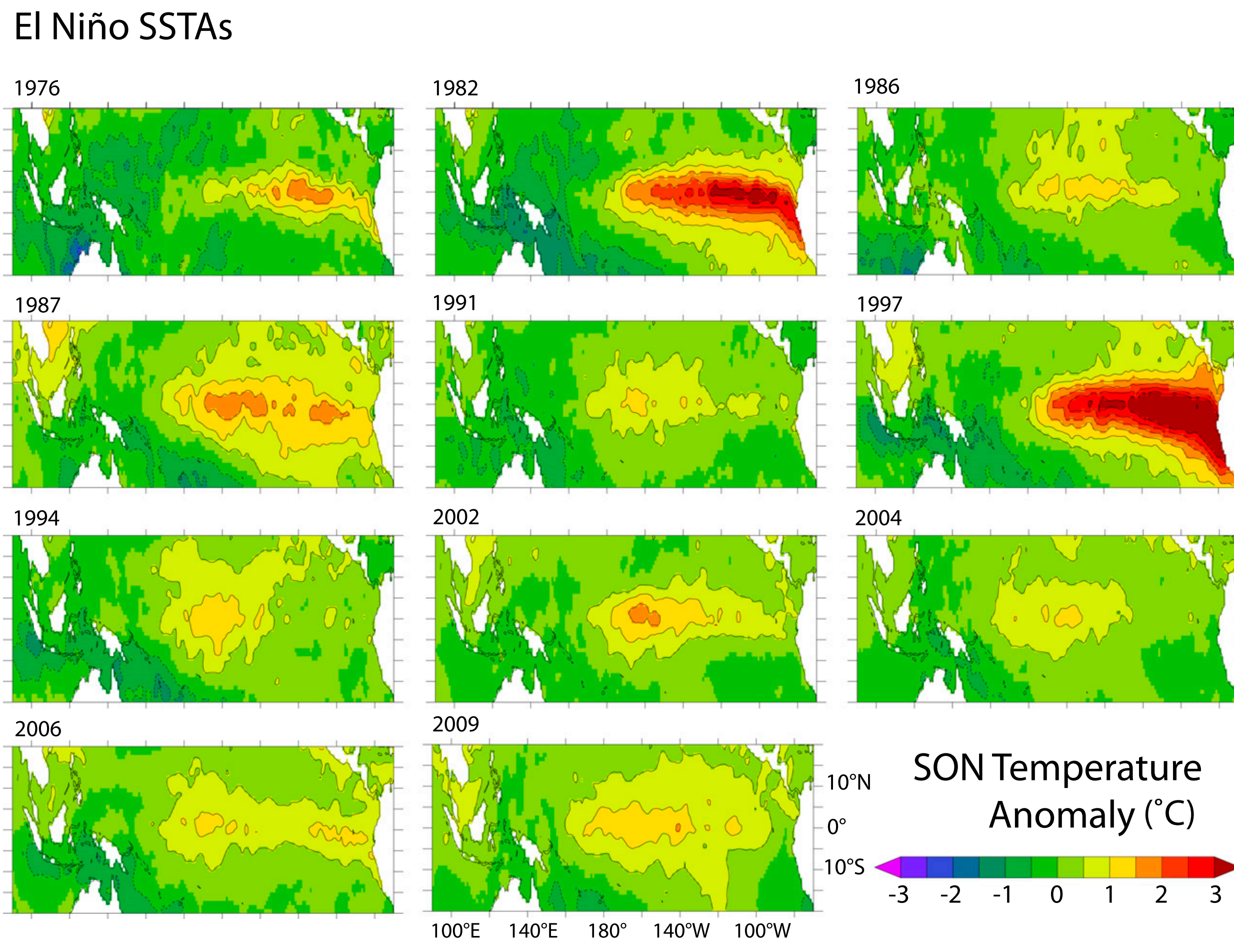

FIG. B1. SON-averaged SSTA in the tropical Pacific in the years with El Niño status based on the NOAA historical ENSO definition (1974–2011).

precipitation anomaly and ENSO SSTAs. If there is a statistically useful linkage between these other events and seasonal precipitation anomaly, it is over significantly fewer regions than seen in the OLR El Niño and OLR La Niña cases (Australia appears to be one region where useful non-OLR El Niño event associations exist).

This work strongly suggests that there are immediately realizable benefits to using OLR behavior to identify the tropical Pacific events that are most likely to influence seasonal weather anomalies on a global scale. Notably, our OLR-based indices offer a method for clearly detecting, in what is currently a subset of the commonly identified ENSO years, when increased levels of confidence can be placed in year 0/1 DJF and later ENSO-type seasonal forecasts.

Our results apply to the majority of the regions strongly affected by ENSO. However, when interest is in a specific region, it is always prudent to carefully consider as much of the relevant and available information as possible, including the use of other indices. We must leave it to the seasonal forecasting community to decide how best to employ our results to further specific national forecast objectives.

The results here have been obtained over the full period for which OLR information is available. It should be recognized, however, that ENSO has been documented to exhibit considerable changes in behavior from one multidecadal period to the next (e.g., Harrison and Chiodi 2015). Although the good correspondence between the OLR-event composites and previous-period work of Ropelewski and Halpert (1987, 1989) suggests many aspects of the associated precipitation patterns have been stable for about a century, it will require monitoring to see the extent to which the OLR relationships and details of the OLR behavior (e.g., discontinuities in OLR distribution) observed over the recent decades hold in the future.

The mechanisms responsible for the different behavior of SSTA- and OLR-based indices and the global

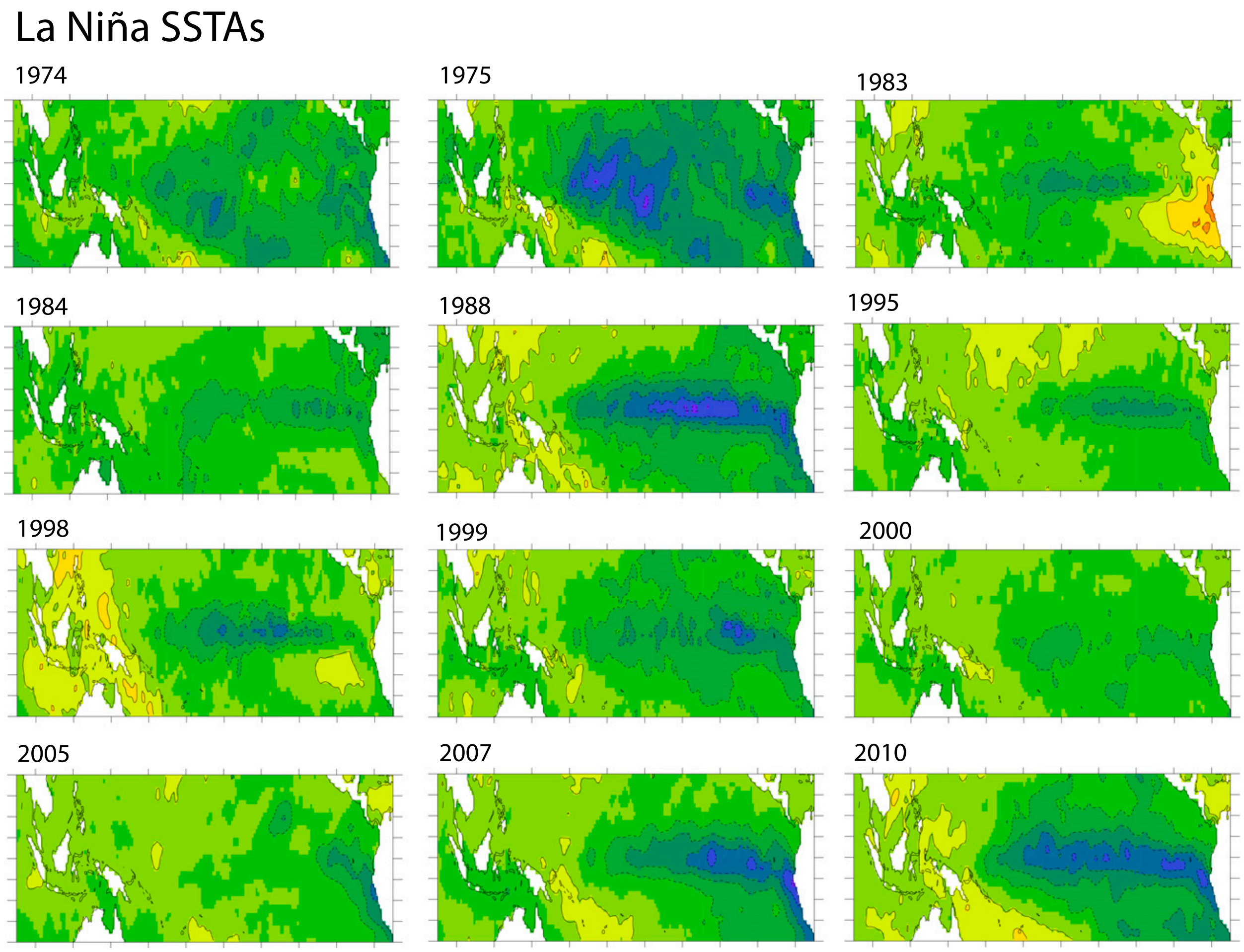

FIG. B2. SON-averaged SSTA in the tropical Pacific in the years with La Niña status based on the NOAA historical ENSO definition (1974–2011).

weather anomalies associated with ENSO events merit additional research. Clearly, the coupled tropical ocean–atmosphere system behaves differently in its OLR behavior than in its SSTA behavior. When understanding the large-scale seasonal patterns of anomalous precipitation is the goal, understanding tropical Pacific OLR behavior is important. Short-term subseasonal zonal wind events and their connection to OLR anomalies appear to be an important factor linking OLR and SSTA, and models that include these processes realistically may offer both improved understanding and improved forecast skill in the future.

Acknowledgments. This publication is partially funded by the Joint Institute for the Study of the Atmosphere and Ocean (JISAO) under NOAA Cooperative Agreement NA10OAR4320148 and by support from the Climate Observations Division of the NOAA Climate Program Office as well as from NOAA's Pacific Marine Environmental Laboratory. We thank the three anonymous reviewers for their time and comments, which have led to improvements in this paper. We thank S. Bigley for proofreading this manuscript for us.

APPENDIX A

Comparison of HIRS and NOAA Interpolated OLR Datasets

Our results are mainly based on the Advanced Very High Resolution Radiometer (AVHRR)-based NOAA interpolated dataset of Liebmann and Smith (1996), which is available starting in 1974. For the post-1979 period, daily averages of OLR on a $1^\circ \times 1^\circ$ grid are also available from the HIRS-based NOAA OLR climate dataset (Lee et al. 2007). With respect to our purposes, the two datasets closely agree with one another; the

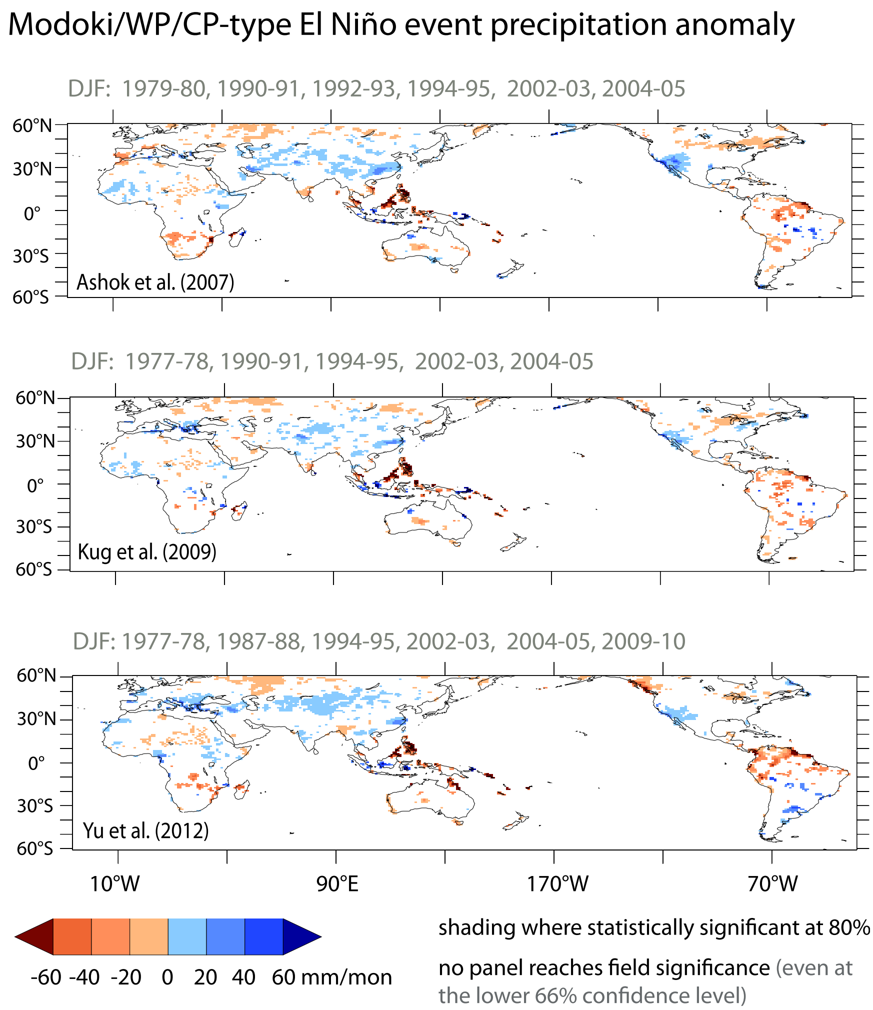

FIG. C1. DJF precipitation anomaly composites based on the years listed above each panel, which are the non-OLR years identified as El Niño Modoki, WP El Niño, and CP El Niño by Ashok et at. (2007), Kug et al. (2009), and Yu et al. (2012), respectively. None are field significant.

OLR El Niño index based on each dataset is plotted in Fig. A1 for comparison purposes. We expect that the HIRS dataset will provide a useful addition to ENSO-monitoring capability. We focus on the AVHRR OLR dataset here, since it is the longer record.

APPENDIX B

Tropical Pacific SSTAs

The 3-month average tropical Pacific SSTAs seen during September through November (year 0) of the years with ENSO status based on the NOAA definition are shown in this appendix for reference. The years identified as El Niño by the NOAA (SSTA based) definition are shown in Fig. B1 and the La Niña years in Fig. B2. The OLR indices for ENSO discussed herein identify the OLR ENSO events by the beginning of December (year 0) in 9 of 10 cases.

APPENDIX C

Precipitation Anomaly Associations with CP-Type El Niño Years

Here we show DJF precipitation anomaly composites based on the non-OLR El Niño years identified alternatively as Modoki (Ashok et al. 2007), warm pool (Kug et al. 2009), and central Pacific (Yu et al. 2012) El Niño years (Fig. C1). Some similarity in the respective composites can be expected because several of the same years appear in each list (see list of years above each panel of

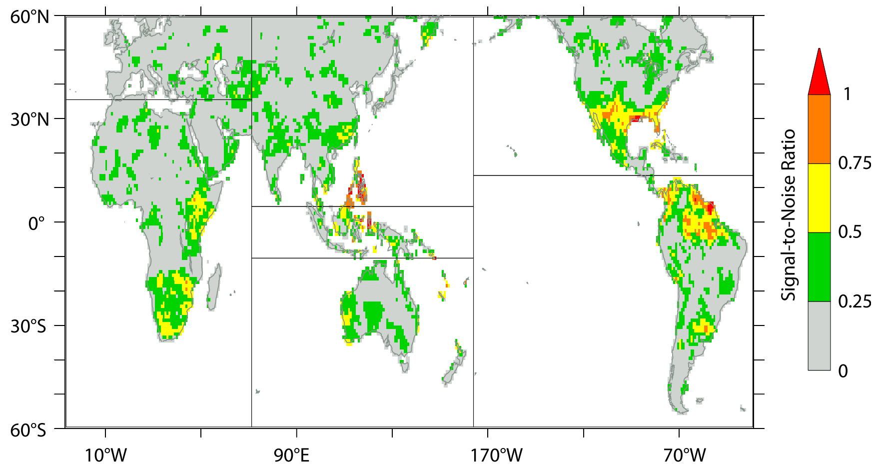

FIG. D1. The signal-to-noise ratio for DJF-averaged land precipitation anomaly based on a linear regression with DJF-averaged Niño-3.4 SSTA.

Fig. C1). Anomalies are shaded in this case where they are statistically significant at the 80% confidence interval, meaning that, on average, 20% of the area should be shaded even in the case that there is no relationship between the index chosen and land precipitation. In each case (Figs. C1a–c) the amount of shaded land area is very close to the amount that should be expected by this null hypothesis (none are field significant).

APPENDIX D

Estimating the Effective Number of Spatial Degrees of Freedom

To estimate the ESDOF contained in DJF-averaged land precipitation anomaly (period 1975–2011), we referred to the two methods discussed by Bretherton et al. (1999). Computing ESDOF over each continent (see boxes in Fig. D1), we find 53 and 70 total ESDOF based on the ''mixed moment'' and ''eigenvalue formula'' methods, respectively. Bretherton et al. (1999) reports that when the number of sampling times is less than a few hundred and not much greater than the ESDOF (as is the case here), the mixed-moment approach is unstable (it exhibits large scatter) and the eigenvalue-formula approach tends to be biased low. This suggests that these estimates are conservative. Further examination has shown that when the ESDOF is computed over smaller regions and summed, larger sums are produced. For example, we find that the eigenvalue formula yields 112, rather than 70 ESDOF, when the total ESDOF is estimated based on considering the tropical and nontropical regions of the larger continents separately. Precision about the ESDOF contained appears to be difficult. Thus, we have computed results over an extended range of possibilities (25–200 ESDOF).

REFERENCES

Ashok, K., S. K. Behera, S. A. Rao, H. Weng, and T. Yamagata, 2007: El Niño Modoki and its possible teleconnection. *J. Geophys. Res.,* **112,** C11007, doi:10.1029/2006JC003798.

Bretherton, C. S., M. Widmann, V. P. Dymnikov, J. M. Wallace, and I. Bladé, 1999: The effective number of spatial degrees of freedom of a time-varying field. *J. Climate,* **12,** 1990–2009, doi:10.1175/1520-0442(1999)012<1990:TENOSD>2.0.CO;2.

Capotondi, A., and Coauthors, 2015: Understanding ENSO diversity. *Bull. Amer. Meteor. Soc.,* doi:10.1175/BAMS-D-13-00117.1, in press.

Chiodi, A. M., and D. E. Harrison, 2008: Characterizing the interannual variability of the equatorial Pacific: An OLR perspective. NOAA Tech. Memo. OAR PMEL-140, NTIS: PB2008-112890, 30 pp. [Available online at http://www.pmel.noaa.gov/pubs/PDF/chio3204/chio3204.pdf.]

——, and ——, 2010: Characterizing warm-ENSO variability in the equatorial Pacific: An OLR perspective. *J. Climate,* **23,** 2428–2439, doi:10.1175/2009JCLI3030.1.

——, and ——, 2013: El Niño impacts on seasonal U.S. atmospheric circulation, temperature, and precipitation anomalies: The OLR-event perspective. *J. Climate,* **26,** 822–837, doi:10.1175/JCLI-D-12-00097.1.

——, and ——, 2015: Equatorial Pacific easterly wind surges and the onset of La Niña events. *J. Climate,* **28,** 776–792, doi:10.1175/JCLI-D-14-00227.1.

——, ——, and G. A. Vecchi, 2014: Subseasonal atmospheric variability and El Niño waveguide warming: Observed effects of the Madden–Julian oscillation and westerly wind events. *J. Climate,* **27,** 3619–3642, doi:10.1175/JCLI-D-13-00547.1.

Garreaud, R. D., and J. M. Wallace, 1998: Summertime incursions of midlatitude air into subtropical and tropical South America. *Mon. Wea. Rev.,* **126,** 2713–2733, doi:10.1175/1520-0493(1998)126<2713:SIOMAI>2.0.CO;2.

Halpert, M. S., and C. F. Ropelewski, 1992: Surface temperature patterns associated with the Southern Oscillation.

J. Climate, **5,** 577–593, doi:10.1175/1520-0442(1992)005<0577:STPAWT>2.0.CO;2.

Harrison, D. E., and N. K. Larkin, 1998: Seasonal U.S. temperature and precipitation anomalies associated with El Niño: Historical results and comparison with 1997–98. *Geophys. Res. Lett.,* **25,** 3959–3962, doi:10.1029/1998GL900061.

——, and A. M. Chiodi, 2009: Pre- and post-1997/98 westerly wind events and equatorial Pacific cold tongue warming. *J. Climate,* **22,** 568–581, doi:10.1175/2008JCLI2270.1.

——, and ——, 2015: Multi-decadal variability and trends in the El Niño-Southern Oscillation and tropical Pacific fisheries implications. *Deep-Sea Res. II,* **113,** 9–21, doi:10.1016/j.dsr2.2013.12.020.

Kiladis, G. N., and H. F. Diaz, 1989: Global climatic anomalies with extremes in the Southern Oscillation. *J. Climate,* **2,** 1069–1090, doi:10.1175/1520-0442(1989)002<1069:GCAAWE>2.0.CO;2.

Kug, J.-S., F.-F. Jin, and S.-I. An, 2009: Two types of El Niño events: Cold tongue El Niño and warm pool El Niño. *J. Climate,* **22,** 1499–1515, doi:10.1175/2008JCLI2624.1.

Kumar, A., B. Jha, Q. Zhang, and L. Bounoua, 2007: A new methodology for estimating the unpredictable component of seasonal atmospheric variability. *J. Climate,* **20,** 3888–3901, doi:10.1175/JCLI4216.1.

Larkin, N. K., and D. E. Harrison, 2002: ENSO warm (El Niño) and cold (La Niña) event life cycles: Ocean surface anomaly patterns, their symmetries, asymmetries, and implications. *J. Climate,* **15,** 1118–1140, doi:10.1175/1520-0442(2002)015<1118:EWENOA>2.0.CO;2.

——, and ——, 2005a: Global seasonal temperature and precipitation anomalies during El Niño autumn and winter. *Geophys. Res. Lett.,* **32,** L16705, doi:10.1029/2005GL022860.

——, and ——, 2005b: On the definition of El Niño and associated seasonal average U.S. weather anomalies. *Geophys. Res. Lett.,* **32,** L13705, doi:10.1029/2005GL022738.

Lee, H.-T., 2014: Outgoing longwave radiation—Daily climate data record algorithm theoretical basis document. NOAA/NCDC Rep. CDRP-ATBD-0526, 46 pp. [Available online at http://www1.ncdc.noaa.gov/pub/data/sds/cdr/CDRs/Outgoing%20Longwave%20Radiation%20-%20Daily/AlgorithmDescription.pdf.]

——, A. Gruber, R. G. Ellingson, and I. Laszlo, 2007: Development of the HIRS outgoing longwave radiation climate dataset. *J. Atmos. Oceanic Technol.,* **24,** 2029–2047, doi:10.1175/2007JTECHA989.1.

Liebmann, B., and C. A. Smith, 1996: Description of a complete (interpolated) outgoing longwave radiation dataset. *Bull. Amer. Meteor. Soc.,* **77,** 1275–1277.

Livezey, R. E., and W. Y. Chen, 1983: Statistical field significance and its determination by Monte Carlo techniques. *Mon. Wea. Rev.,* **111,** 46–59, doi:10.1175/1520-0493(1983)111<0046:SFSAID>2.0.CO;2.

Mastrandrea, M. D., and Coauthors, 2010: Guidance note for lead authors of the IPCC Fifth Assessment Report on consistent treatment of uncertainties. 4 pp. [Available online at https://www.ipcc.ch/pdf/supporting-material/uncertainty-guidance-note.pdf.]

Met Office Hadley Center, 2003: Hadley Centre Sea Ice and Sea Surface Temperature dataset, version 1.1. Accessed 2 March 2012. [Available online at http://www.metoffice.gov.uk/hadobs/hadisst/data/download.html.]

NOAA/NCAR, 1996: NOAA Interpolated Outgoing Longwave Radiation (OLR). NOAA/OAR/ESRL PSD, accessed 20 March 2012. [Available online at http://www.esrl.noaa.gov/psd/data/gridded/data.interp_OLR.html.]

NOAA/NCDC, 2014: NOAA's Outgoing Longwave Radiation–Daily Climate Data Record (OLR–Daily CDR), version 4.2.10. NCDC TDS Installation, accessed 27 October 2014. [Available online at https://www.ncdc.noaa.gov/thredds/dodsC/cdr/olr-daily/olr-daily.ncml.]

Okumura, Y. M., and C. Deser, 2010: Asymmetry in the duration of El Niño and La Niña. *J. Climate,* **23,** 5826–5843, doi:10.1175/2010JCLI3592.1.

Rasmusson, E. M., and T. H. Carpenter, 1982: Variations in tropical sea surface temperature and surface wind fields associated with the Southern Oscillation/El Niño. *Mon. Wea. Rev.,* **110,** 354–384, doi:10.1175/1520-0493(1982)110<0354:VITSST>2.0.CO;2.

Rayner, N. A., D. E. Parker, E. B. Horton, C. K. Folland, L. V. Alexander, D. P. Rowell, E. C. Kent, and A. Kaplan, 2003: Global analyses of sea surface temperature, sea ice, and night marine air temperature since the late nineteenth century. *J. Geophys. Res.,* **108,** 4407, doi:10.1029/2002JD002670.

Ropelewski, C. F., and M. S. Halpert, 1986: North American precipitation and temperature patterns associated with the El Niño/Southern Oscillation (ENSO). *Mon. Wea. Rev.,* **114,** 2352–2362, doi:10.1175/1520-0493(1986)114<2352:NAPATP>2.0.CO;2.

——, and ——, 1987: Global and regional scale precipitation patterns associated with the El Niño/Southern Oscillation. *Mon. Wea. Rev.,* **115,** 1606–1626, doi:10.1175/1520-0493(1987)115<1606:GARSPP>2.0.CO;2.

——, and ——, 1989: Precipitation patterns associated with the high index phase of the Southern Oscillation. *J. Climate,* **2,** 268–284, doi:10.1175/1520-0442(1989)002<0268:PPAWTH>2.0.CO;2.

Rudolf, B., and U. Schneider, 2005: Calculation of gridded precipitation data for the global land-surface using in-situ gauge observations. *Proc. Second Workshop of the International Precipitation Working Group (IPWG),* Monterey, CA, European Organisation for the Exploitation of Meteorological Satellites, 231–247.

——, A. Becker, U. Schneider, A. Meyer-Christoffer, and M. Ziese, 2010: The new "GPCC Full Data Reanalysis Version 5" providing high-quality gridded monthly precipitation data for the global land-surface is publicly available since December 2010. GPCC Status Rep., 7 pp.

Schneider, U., A. Becker, P. Finger, A. Meyer-Christoffer, B. Rudolf, and M. Ziese, 2011: GPCC monitoring product: Near real-time monthly land-surface precipitation from rain-gauges based on SYNOP and CLIMAT data. Accessed 6 April 2012, doi:10.5676/DWD_GPCC/MP_M_V4_100.

Smith, S. R., D. M. Legler, M. J. Remigio, and J. J. O'Brien, 1999: Comparison of 1997–98 U.S. temperature and precipitation anomalies to historical ENSO warm phases. *J. Climate,* **12,** 3507–3515, doi:10.1175/1520-0442(1999)012<3507:COUSTA>2.0.CO;2.

Trenberth, K. E., G. W. Branstator, D. Karoly, A. Kumar, N.-C. Lau, and C. Ropelewski, 1998: Progress during TOGA in understanding and modeling global teleconnections associated with tropical sea surface temperatures. *J. Geophys. Res.,* **103,** 14 291–14 324, doi:10.1029/97JC01444.

Wheeler, M. C., and H. H. Hendon, 2004: An all-season real-time multivariate MJO index: Development of an index for monitoring and prediction. *Mon. Wea. Rev.,* **132,** 1917–1932, doi:10.1175/1520-0493(2004)132<1917:AARMMI>2.0.CO;2.

Wolter, K., R. M. Dole, and C. A. Smith, 1999: Short-term climate extremes over the continental United States and ENSO. Part I: Seasonal temperatures. *J. Climate,* **12,** 3255–3272, doi:10.1175/1520-0442(1999)012<3255:STCEOT>2.0.CO;2.

Yu, J.-Y., Y. Zou, S. T. Kim, and T. Lee, 2012: The changing impact of El Niño on US winter temperatures. *Geophys. Res. Lett.,* **39,** L15702, doi:10.1029/2012GL052483.